Radiochemical analysis of cadmium in nitric and phosphoric acid

Thesis for the Master's degree in Chemistry

Håvard Kristiansen

Faculty of Mathematics and Natural Sciences

UNIVERSITY OF OSLO

May 2015

Abstract

The goal of this research project was to find a way to produce fertilizer with low concentrations of cadmium from phosphate rock with relatively high cadmium concentrations. A method for the production of a radioactive cadmium tracer was developed and implemented. The tracer was used to investigate how cadmium behaves in a critical step of a process for fertilizer production. A method for measuring the radioactivity from ^{109}Cd was developed, tested and implemented. The ^{109}Cd radiotracer and the detection method were used to investigate solvent extraction from nitric and phosphoric acid, as well as from an industrial fertilizer-production solution. After a screening of a selection of possible commercial extractants, di-(2-ethylhexyl)phosphoric acid (HDEHP) and di-(2,4,4-trimethyl pentyl)dithiophosphinic acid (Cyanex 301) where studied closely. The results were interpreted in order to propose chemical equations for how HDEHP and Cyanex 301 react with cadmium and the acid matrix.

Acknowledgements

I wish to thank my main supervisors Jon-Petter Omtvedt and Dag Eriksen, who have always been enthusiastic about what we could achieve together and who have showed confidence in my potential and abilities. I am grateful for the time and resources you have laid down so that I could complete this work. I would also like to thank my co-supervisors Grethe Wibetoe and Tom Andersen, who offered me their help and guidance even though I did not have a background in their respective areas of expertise. I would also like to thank Siri Simonsen at the department of Geosciences who kindly performed an ICP-MS analysis for me. I would also like to thank my fellow students for our helpful discussions and generally collegial atmosphere.

I would also like to thank Tom Rames Jørgensen at Yara for answering my questions about how they make fertilizer. I have found motivation in working with something that is relevant to both global food production and Norwegian industry.

I am very grateful to my family for all their help these past two years. And last, but more than anyone else, I thank my wife for being awesome in every way. I could not have done this without you.

List of special terms and abbreviations

Cyanex 301	Di-(2,4,4-trimethyl pentyl)dithiophosphinic acid
FAO	Food and Agriculture organization of the United Nations
HA	Generalized monoprotic extractant
HDEHP	Di-(2-ethylhexyl)phosphoric acid
HPGe	High-purity Germanium
LSC	Liquid Scintillation Counting
LSC-cocktail	A solution consisting of an organic solvent, a surfactants and a scintillating compound. It is used to measure the radioactivity content in solutions.
Mother liquor	A solution of phosphate rock in nitric acid. After precipitation of $Ca(NO_3)_2$ From the process Yara uses to produce fertilizer.
NP-fertilizer	Nitrogen and phosphate fertilizer
NPK-fertilizer	Nitrogen, phosphate and potassium fertilizer
PMT	Photomultiplier tube
rpm	Rotations per minute
$T_{1/2}$	Half-life of a radionuclide
TBP	Tri-butyl phosphate
λ	Decay constant of a radionuclide

Contents

1 Introduction

1.1 Phosphate fertilizer and food security

One of the greatest challenges the modern global society faces is to provide enough food for everyone. The Food and Agriculture Organization (FAO) of the United Nations estimates that global food production must increase by 70% by 2050. According to the FAO, most of that increase will need to come from higher crop yields from farmland already in use [2].

The role of fertilizers in agriculture is to provide one or more plant nutrients to the soil. A plant nutrient is any chemical element required by the plant in order to have a normal life cycle [3]. There are two categories of nutrients; macronutrients and micronutrients. Macronutrients form the main building blocks of plant tissue, and are therefore required in large quantities. Carbon, hydrogen, oxygen, nitrogen, phosphorus, sulfur, potassium, calcium and magnesium are macronutrients. Of these, nitrogen, phosphorous and potassium are most commonly applied to the crops through fertilizers, either as so-called straight fertilizers, which only provide one of the nutrients, or as compound fertilizer such as NP, PK or NPK, which contain a mixture of the different elements.

Fertilizers play a crucial role in modern agriculture. Estimates of the portion of global crop-yield that is attributable to the use of fertilizer range from 40 to 60% [4]. Therefore, fertilizer will probably be essential in attaining the required rise in food production. However, the raw material for phosphate fertilizer, phosphate rock, is not a renewable resource. It is formed in geological processes, either as sediments from seawater or as magma in volcanic eruptions [5]. Therefore, global food-production depends on the remaining reserves of phosphate rock to cover the future demand of phosphate fertilizer until a renewable source of phosphate is developed.

Phosphate rock contains large portions of the mineral apatite. There are three main versions of apatite: Fluoroapatite ($Ca_5(PO_4)_3F$), hydroxyapatite ($Ca_5(PO_4)_3OH$) and chlorapatite ($Ca_5(PO_4)_3Cl$). Plants generally absorb nutrients through their roots. For a nutrient to become available to the roots, it must dissolve into the water around the roots. Apatite is insoluble in water, so to produce a phosphate fertilizer that quickly delivers phosphate to crops, one must convert the phosphate (PO_4^{3-}) in the apatite to the more soluble hydrogen phosphate (HPO_4^{2-}) or dihydrogen phosphate ($H_2PO_4^-$). There are several ways to do so and several kinds of phosphate fertilizers.

Natural deposits of apatite normally contain heavy metals, such as arsenic (As), cadmium (Cd), chromium (Cr), lead (Pb), mercury (Hg) and uranium (U). There are concerns that as the reserves of available clean phosphate rock deposits dwindle, the industry will have to turn to reserves which

were previously considered too impure [6]. In light of this and in order to avoid contamination of croplands, many countries have established upper thresholds on the allowed concentrations of heavy metals in fertilizers.

The history of cadmium makes it a well-known example of the toxicity of heavy metals. In the twentieth century, many villagers in the Toyama Prefecture in Japan experienced a gruesome illness later known as the "Itai-Itai Disease" ("Ouch-ouch disease") [7]. Symptoms included bone pains, osteomalacia (a softening and increased fragility of the bones), miscarriages, infertility and renal failure. Patients usually drank from and ate rice watered by the Jinzu River. Upstream from where the disease occurred was a mine where cadmium, zinc and lead was excavated. Wastewater laden with the three heavy metals flowed into the river, and researchers later concluded that the Itai-Itai Disease was in fact a widespread example of chronic cadmium poisoning. There is little doubt that the story of the Itai-Itai disease serves as a warning against allowing high levels of cadmium in food and drinking water.

1.2 Ethical and social aspects

In addition to possible heavy metal contamination, the use and production of fertilizers may have other negative effects on the environment. This section reviews some of those issues and discusses the ethical challenges involved in conducting a research project which may cause prolonged or increased production and use of fertilizers.

Phosphate is an important and often limiting nutrient to algae in natural waters. Run-off from fertilized croplands may increase the flux of phosphates to water basins, thereby accelerating the growth of algae. When the algae die, they sink to the bottom of the basin, where they are decomposed by bacteria. The decomposition requires oxygen, so increasing amounts of algae will deplete the oxygen in the water, and may eventually make the conditions intolerable for oxygen-dependent animals such as fish. This process of oxygen depletion and algae bloom in natural waters is called eutrophication. Globally, fertilizer run-off is the largest cause of eutrophication, followed by municipal sewage-discharges [8].

The most common way to use fertilizer is to apply only macronutrients such as nitrogen, phosphorus and potassium. However, plants and animals rely on small amounts of micronutrients as well, such as zinc, copper, manganese and iron. Use of macronutrient fertilizer may give large crops in the short run, but if those large crops absorb all the micronutrients in the soil, crop fertility may decrease in the long run, and the land may become infertile for future generations.

The effects of both eutrophication and micronutrient depletion depend on several factors such as fertilizer application-rates and soil composition in and around the farmland. One can hope that competent and responsible use may decrease those effects to a level where the enhanced crop yields justify the extra burden on nature and does not rob future generations of fertile land.

Fertilizer production requires mining of phosphate rock. Phosphate rock is usually mined from strip-mines, which means removing all the soil and rock above the mineral deposits, thereby destroying the ecosystem in the mined area. Fertilizer production also requires large amounts of energy. Ammonia production alone, of which 83 % goes to fertilizer production, requires about 1.4 % of the global energy consumption [9]. The associated greenhouse gas emissions are considerable. In addition, fertilizers emit nitrous oxide (N_2O) and CO_2 when they are applied to croplands. According to the International Fertilizer Industry Association, production, distribution and use of fertilizers cause 2-3% of the global emission of greenhouse gasses. On the other hand, all human activities burden the environment, and the importance of fertilizers for food production may justify the toll it takes on the environment.

Humans and animals excrete most of the phosphate they ingest. Consequently, most of the phosphate that is put into fertilizers today will eventually end up in sewage water and finally dissolve in the oceans. If society could replace this wasteful practice with a system where phosphorus is recycled back to croplands, it may avoid many of the above mentioned issues with phosphate fertilizers. Traditional use of manure is one way of recycling phosphate, but the use of manure alone has not been able to compete with the use of commercial fertilizers.

Some creative and promising projects are underway in order to recycle phosphate. For example, urine-diverting toilets facilitate the use of urine as fertilizer [10]. Another approach involves the extraction of phosphate from municipal sewage water [11]. However, development and implementation of such technologies on a sufficiently large scale takes time as well as economic and political dedication. In the meantime, the global food supply will have to rely on fertilizer produced from phosphate rock.

1.3 Project goals

The goal of this research project was to find a way to produce fertilizer with low concentrations of cadmium from apatite with high concentrations of cadmium. These investigations were to be performed by using radiochemical methods. The following sub-goals were established to achieve this:

Goal 1: To produce a radioactive cadmium tracer, using the cyclotron at the Oslo Cyclotron Lab. It is possible to by ^{109}Cd commercially, but it is expensive to do so. Therefore, and because it provided a good opportunity to build experience in practical radiochemistry, this goal was included in the project.

Goal 2: To measure how cadmium behaves in selected steps of a fertilizer production-process, using the radioactive tracer produced in Goal 1.

Goal 3: To find an effective extractant for cadmium, so that solvent extraction could be used to remove cadmium from a process solution in the fertilizer production-process. Ideally, the extractant should extract cadmium and other toxic metals, but not calcium or other non-toxic metals which are abundant in the process solution. If a promising extractant was discovered, an industrial process using that extractant should be outlined.

1.4 Why use radiochemistry?

A radiotracer is a radioactive atom, ion or molecule that that allows researchers to track a species through a process by measuring the radiation emitted by the radiotracer. There are numerous industrial and research-related applications of radiotracers. Techniques for detecting ionizing radiation generally have low detection limits. Picograms (10^{-12} g) or less of radioactive material is usually detectable with conventional detectors. Therefore, researchers may use so small amounts of the tracer compound that its addition does not alter the process under investigation.

The radioactive nature of a nucleus is not affected by external factors such as chemical bonds, pressure or temperature. A stable and a radioactive isotope of the same element will generally share the same physicochemical behavior, which means that the radiation from the radioactive isotope can show how all the atoms of that element, radioactive or not, behave chemically or mechanically in the system under investigation. Another advantage of radiotracer analysis is that it often offers easy sample preparation, compared to other analytical techniques.

2 Background and theory

2.1 Production of nitro-phosphate fertilizer

The Odda process is a production process for nitro-phosphate fertilizer. The process was invented in Odda, Norway in 1927 and the Norwegian fertilizer producer Yara still uses it. The following paragraphs provide a brief description of the process.

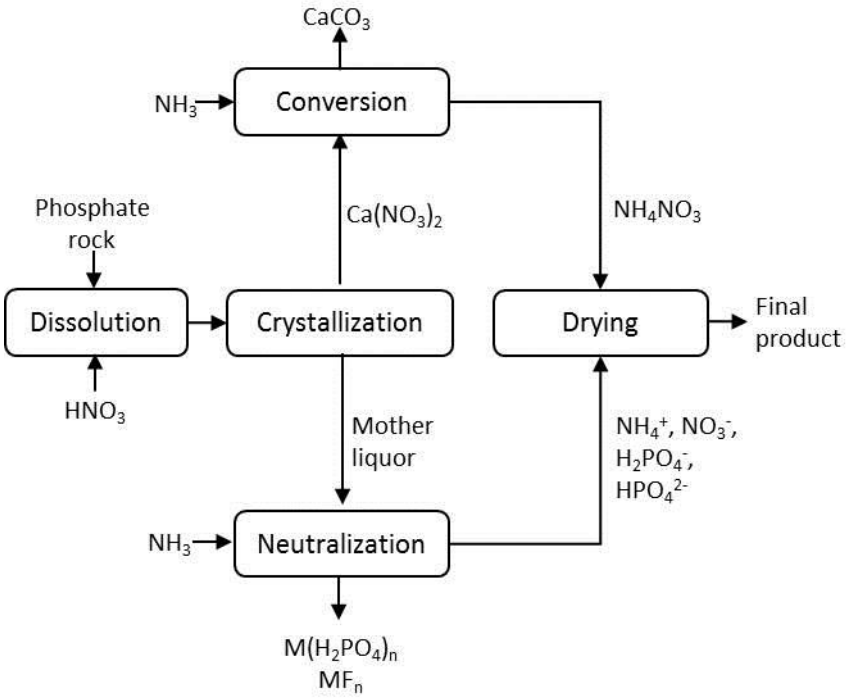

Figure 1: Sketch of the steps involved in the Odda process for the production of nitro-phosphate fertilizer. The figure was drawn based on the information in reference [3].

2.1.1 Step 1: Dissolution of rock

The first step is to grind the rock and dissolve it in excess nitric acid:

$$Ca_5(PO_4)_3F\,(s) + 10HNO_3\,(aq) \rightarrow 5Ca(NO_3)_2\,(aq) + 3H_3PO_4\,(aq) + HF\,(g) \qquad \text{Eq. 1}$$

The heat of reaction raises the temperature in the solution to 50-70 °C. This causes a portion of the hydrofluoric acid to evaporate.

2.1.2 Step 2: Precipitation of calcium nitrate

Step 2 involves slowly cooling the solution to as low as -5°C to precipitate about 80-85% of the calcium as calcium nitrate:

$$Ca(NO_3)_2(aq) + 4H_2O \rightarrow Ca(NO_3)_2{\cdot}4H_2O(s) \quad \text{Eq. 2}$$

Calcium nitrate is filtered out and marketed either as a nitrate fertilizer or as a means to avoid sulfide-generation in sewage water. It can also be contacted with ammonia to produce ammonium nitrate and calcium carbonate (the conversion stage in Figure 1).

2.1.3 Step 3: Neutralization of mother liquor

After removal of calcium nitrate, the process solution contains phosphoric acid, nitric acid, hydrofluoric acid, calcium and magnesium nitrates, dissolved cations such as iron, aluminum and silicon, and suspended particles such as quarts. Yara calls this solution mother liquor. This acidic solution is neutralized with gaseous ammonia under strict pH control. Nitric acid is the strongest acid present and is therefore the first species which reacts during neutralization:

$$HNO_3\,(aq) + NH_3(g) \rightarrow NH_4NO_3\,(aq) \quad \text{Eq. 3}$$

During addition of ammonia, pH increases. If pH gets above approximately 1 (Figure 2), dihydrogen phosphate salts of various metals precipitate:

$$Ca(NO_3)_2\,(aq) + 2H_3PO_4\,(aq) + 2NH_3(g) \rightarrow 2NH_4NO_3\,(aq) + Ca(H_2PO_4)_2\,(s) \quad \text{Eq. 4}$$

Metal fluorides can also precipitate. Yara currently adds just the right amount of ammonia, so that no precipitation occurs. However, precipitation may be part of a future process to separate metals from the solution.

2.1.4 Step 4: Drying, granulation and prilling

In the final part of the production process, water is evaporated from the nitro-phosphate solution to produce a slurry of ammonium hydrogen phosphate, which is made into granules and eventually into smaller prills of the final product. If the final product is supposed to be an NPK fertilizer, potassium chloride or sulfide is added to the solution before it solidifies.

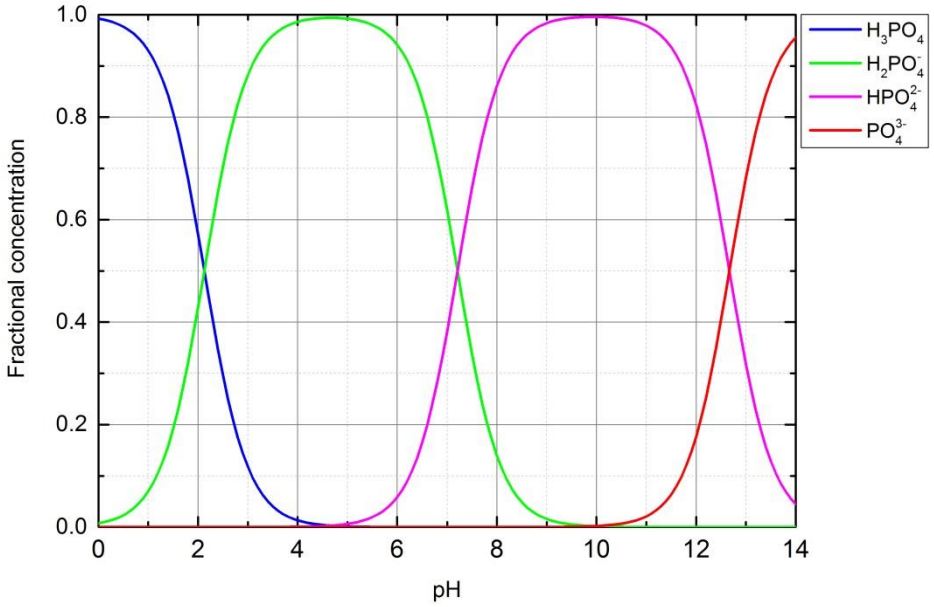

Figure 2: The fractional concentrations of H_3PO_4, $H_2PO_4^-$, HPO_4^{2-} and PO_4^{3-} as functions of pH. The fractional concentration of a species equals the concentration of that species divided by the sum of the concentrations of all the species. The function was plotted based on the pK_a-values in reference [12].

2.2 Cyclotrons and radionuclide production

A cyclotron is a machine that is able to produce intense, high-velocity beams of ions. In theory, it consists of two hollow electrodes in the shape of Ds with the flat ends facing each other (Figure 3). In reality the machines are somewhat more complex in shape and construction, but such details are beyond the scope of this thesis. At the center of the cyclotron there is an inlet from an ion source. The space between the electrodes is called the acceleration gap because there is an electric field across it. Once an ion exits the ion source outlet, it feels the force from the electric field and is accelerated towards one of the electrodes. When the ion exits the acceleration gap, it enters a magnetic field which is directed perpendicularly to the plane of the electrodes and the ion source. The magnetic field makes the ion turn in a semi-circle until it re-enters the acceleration gap. By the time the ion re-enters the acceleration gap, the electric field has switched direction, causing the ion to accelerate towards the other electrode, where it is once more turned around, and so on. As the ion gains speed, the radius of its trajectory increases until it has the desired speed and is deflected out of the cyclotron and onto a target. Typically, the ions will complete around 300 turns. Since the magnetic field is fixed, the cyclotron can simultaneously accelerate ions independently of their attained energy, thereby generating a fixed current of ions.

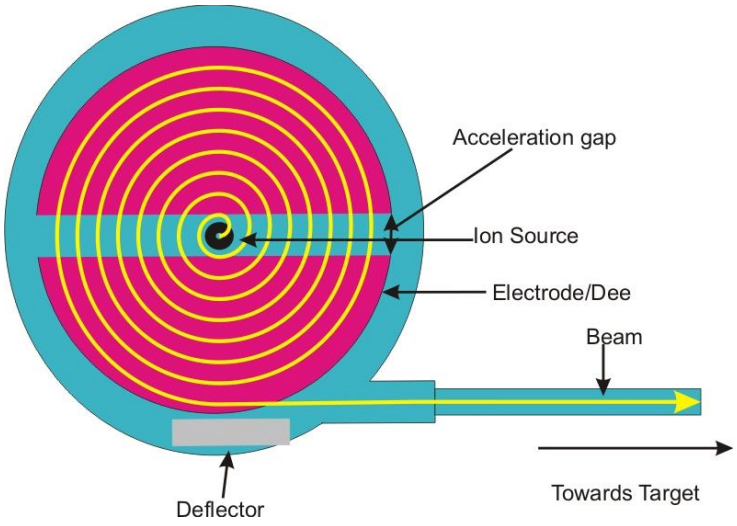

Figure 3: Principle sketch of a cyclotron (a real machine is somewhat more complicated). The ion source outlet is marked in black in the center of the cyclotron. The magnetic field is perpendicular to the paper plane [13].

Cyclotrons are commonly used to induce nuclear reactions by making a projectile nucleus collide with a target nucleus. The target nucleus is contained in a stationary material, onto which the particle beam is directed. When a projectile nucleus approaches a target nucleus, there is a given probability that the two will collide. This probability is described by a term called the cross-section. Cross sections are given in the unit barn, where 1 barn = 10^{-24} cm^2. The cross section is the equivalent of the sizes of the target and projectile nuclides as viewed along the axis between them. However, it does not only describe the geometrical likelihood of hitting a target nucleus, but takes into account the probability that a given nuclear reaction actually will take place. The likelier the reaction, the greater the cross-section.

2.3 Production of ^{109}Cd

The radioactive cadmium isotope ^{109}Cd was selected as the radioactive tracer, because it has a relatively long half-life of 462 days, which meant that once a batch of it had been made, it would remain available for the duration of the project (two years), i.e. the radioactivity concentration would be high enough for the ^{109}Cd to be detected and therefore useful as a radiotracer. Another advantage of using ^{109}Cd as a radioactive tracer is that the radiation it emits can be measured both with liquid scintillation counting (LSC) and gamma spectroscopy.

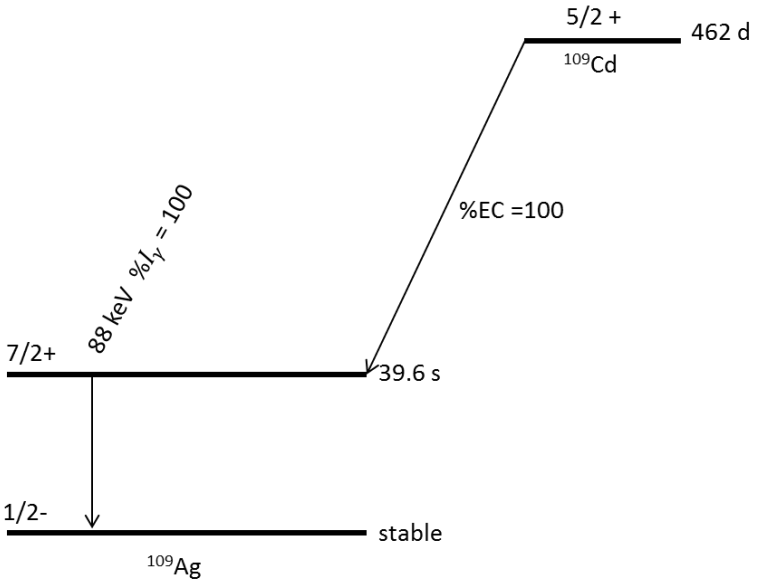

Figure 4: Decay scheme of ^{109}Cd. 100% of ^{109}Cd-desintegrations occur by electron capture to metastable ^{109m}Ag, which in turn decays by internal transition to stable ^{109}Ag. The half-life of ^{109m}Ag is 39.6 s and the internal transition γ-photon carries 88 keV of energy. Simplified from reference [14].

^{109}Cd decays radioactively by a process known as electron capture (Figure 4). Electron capture is a process by which a proton-rich nucleus captures an orbital electron (e^-) and combines it with one of its protons, producing a neutron and a neutrino (ν) [15]. The product nucleus therefore has one proton less and one neutron more than the reactant nucleus. In the decay of ^{109}Cd, the product nucleus is ^{109m}Ag:

$$^{109}Cd + e^- \rightarrow {}^{109m}Ag + \nu \qquad \text{Eq. 5}$$

The neutrino ν that ^{109}Cd emits is not detectable in any practical way. ^{109m}Ag has a short half-life of only 39.6 seconds. ^{109m}Ag is an excited state of stable ^{109}Ag, and can give up its excitation energy by either γ-emission or electron conversion. In γ-emission, the excitation energy is emitted as a photon. In electron conversion, the nucleus excitation energy is transferred to an orbital electron, ejecting the electron from its orbital with a kinetic energy equal to the difference between the nucleus excitation-energy and the orbital binding energy. The emitted electrons have discrete energies of several kilo-electron volts (keV). They are a form of ionizing radiation, and can be detected with radiometric techniques, such as liquid scintillation counting.

When a conversion electron is emitted from a low-lying shell of an atom, an electron from a higher-energy shell will fill the resulting hole in the electron structure. The electron that goes from a high

shell to a low shell loses potential energy in the process. The potential energy can be given of either as an x-ray photon or as an Auger electron. In Auger electron emission, an atomic electron absorbs the potential energy difference, obtaining a kinetic energy equal to the potential energy difference minus its binding energy. The absorbed kinetic energy makes the electron shoot out from the atom, becoming a kind of ionizing radiation.

Natural silver contains two isotopes: 51.83 % ^{107}Ag and 48.17 % ^{109}Ag. ^{107}Ag can react with ^{4}He to produce ^{109}In:

$$^{107}\text{Ag} + {}^{4}\text{He} \rightarrow {}^{109}\text{In} + 2n \qquad \text{Eq. 6}$$

The short-hand way to describe this reaction is ^{107}Ag(α,2n)^{109}In. ^{109}In is radioactive and has a half-life of 4.2 hours. It decays to ^{109}Cd via either electron capture or beta emission.

$$^{109}\text{In} \rightarrow {}^{109}\text{Cd} \quad (T_{1/2} = 4.2 \text{ hours}) \qquad \text{Eq. 7}$$

Because ^{109}In is so short lived compared to ^{109}Cd, practically all the ^{109}In decays to ^{109}Cd in a couple of days after irradiation. A radionuclide disintegrates to 0.1 % of its initial amount in 10 half-lives. When a radionuclide has disintegrated to an undetectable amount, it is said to have “died out”.

^{109}Ag reacts with ^{4}He-projectiles in a similar manner as ^{107}Ag does:

$$^{109}\text{Ag} + {}^{4}\text{He} \rightarrow {}^{111}\text{In} + 2n \qquad \text{Eq. 8}$$

^{111}In has a half-life of 2.8 days and therefore takes about four weeks to die out. ^{111}In decays to non-radioactive ^{111}Cd. Table 1 summarizes the properties ^{109}Cd, ^{109}In and ^{111}In.

Table 1: List of relevant radionuclides, the reactions by which they are produced in this experiment and their relevant properties [1]. ϵ stands for electron capture. β^+ stands for positron emission.

Radionuclide	Production reaction	Decay mode	Half-life	Gamma energy (keV)	Gamma-emissions per 100 decays
^{109}In	^{107}Ag(α,2n)^{109}In	ϵ,β^+	4.2 hours	203.5	74
^{111}In	^{109}Ag(α,2n)^{111}In	ϵ	2.8 days	245.4 171.3	94 90
^{109}Cd	^{109}In → ^{109}Cd	ϵ	462 days	88	3.6 ± 0.1

Several researchers have reported the cross-section of the ^{107}Ag(α, 2n)^{109}In-reaction [16-19]. The reports indicate that the cross-section is at maximum when the incoming ^{4}He-particles have a kinetic energy in the range 25-30 MeV (Figure 5).

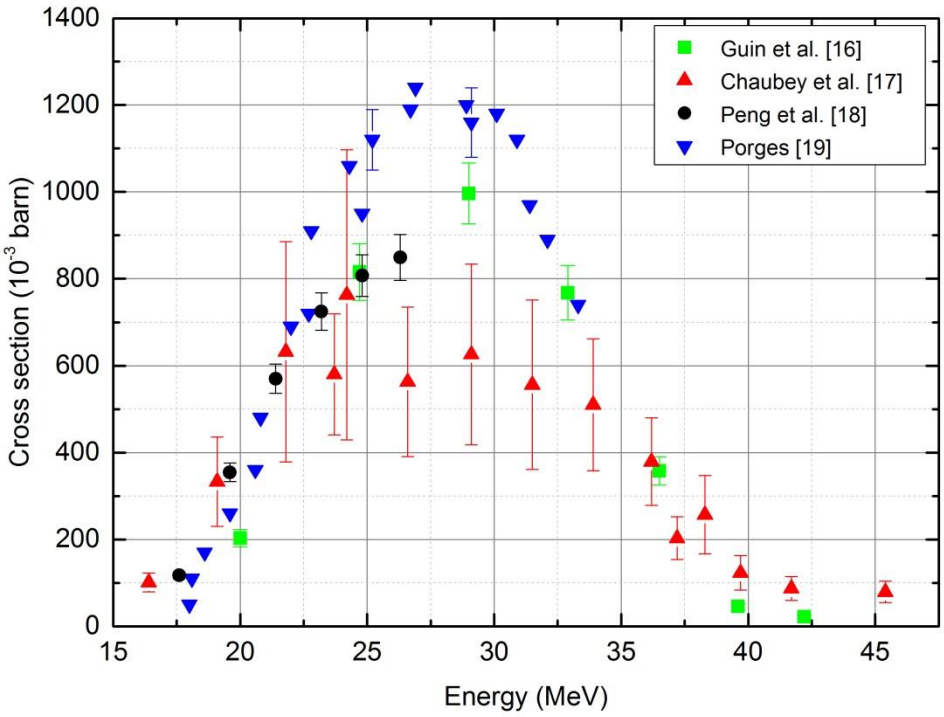

Figure 5: The cross section of the reaction ^{107}Ag(α, 2n)^{109}In as a function of energy, as reported by references [16-19].

2.4 Solvent extraction of cadmium from nitric- and phosphoric acid medium

Solvent extraction is a technique for the extraction and separation of metals. It was developed in the 1940s as a part of the effort to produce pure uranium from uranium ore. Solvent extraction has played a role in nuclear industry ever since, and it has become an important technique for the

reprocessing of spent nuclear fuel. Since the 1960s, solvent extraction has found its uses in the extraction of other valuable metals as well, such as copper, gold and the rare earth elements. It is also used in analytical chemistry, wastewater treatment and various other fields [20] .

Table 2: Extractants discussed in this work.

Systematic name	**Trade name/ acronym**	**Structure**
di-(2-ethylhexyl)phosphoric acid	HDEHP	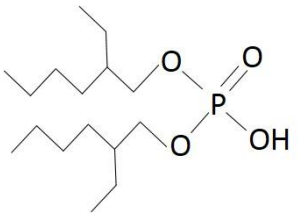
Tributyl phosphate	TBP	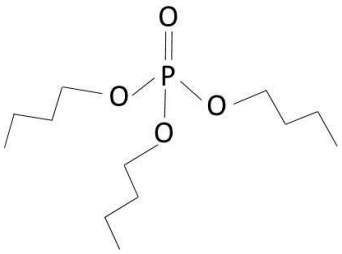
A mixture of: Trihexylphosphine oxide, dihexylmonooctyl-phosphine oxide, dioctylmonohexyl-phosphine oxide and trioctylphosphine oxide	Cyanex 923	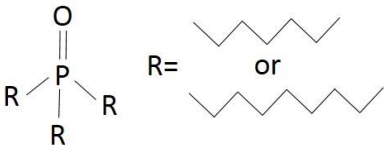
Di-(2,4,4-trimethylpentyl)dithiophosphinic acid	Cyanex 301	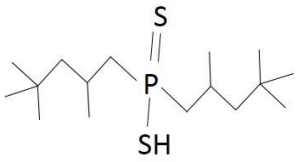
Di-(2,4,4-trimethyl pentyl)phosphinic acid	Cyanex 272	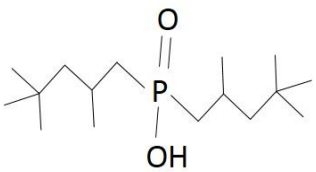

When using solvent extraction, one usually starts with an aqueous solution containing a metal of interest. This is called the feed solution. The feed solution is mixed with an organic solution consisting of an active compound called an extractant dissolved in an inert diluent. Over the years, a wide range of extractants has been developed. They generally function by binding to the metal ion

and forming a complex which is soluble in the organic diluent. The result is a transport of metal from the aqueous phase to the organic phase when the two phases mix. After mixing, the phases usually separate by way of their difference in densities and chemical properties.

For a given metal, the distribution ratio, D, is defined as the concentration of the metal in the organic phase ($[Cd]_{org}$) divided by the concentration in the aqueous phase ($[Cd]_{aq}$):

$$\mathrm{D}_{Cd} = \frac{[\mathrm{Cd}]_{org}}{[\mathrm{Cd}]_{aq}} \qquad \text{Eq. 9}$$

The distribution ratio is used to quantify the degree of extraction of a metal. Alternatively, researchers often report the percent extracted, which is the percentage of the metal atoms which are present in the organic phase at equilibrium after extraction. If the volumes of the aqueous and organic phases are equal, the percent extracted, $\%\mathrm{E}_{Cd}$, is related to the distribution ratio by the following formula:

$$\%\mathrm{E}_{Cd} = 100\% \cdot \frac{\mathrm{D}_{Cd}}{1 + \mathrm{D}_{Cd}} \qquad \text{Eq. 10}$$

The distribution ratio usually depends on several variables, such as pH, extractant concentration, the relative volumes of the phases, temperature etc. Many cation extractants are acids, such as carboxylic acids or organophosphoric esters. They contain an acidic hydrogen atom which they can exchange for a metal cation. They are therefore called cation exchangers. Multivalent cations can bind several extractant molecules. Generally, the extraction of cadmium by a monoprotic extractant HA can be described as [21]:

$$Cd^{2+}\,(aq) + n\mathrm{HA}\,(org) \rightleftharpoons CdA_2(HA)_{(n-2)}\,(org) + 2H^+\,(aq) \qquad \text{Eq. 11}$$

Cation exchangers usually give higher distribution ratios when pH increases, because to increase pH is the same as to reduce the concentration of H^+, which causes the equilibrium in Eq. 11 to shift to the right.

The reaction constant for the reaction in Eq. 11 is:

$$K = \frac{\left[\mathrm{CdA_2(HA)_{(n-2)}}\right][\mathrm{H^+}]^2}{[\mathrm{Cd^{2+}}][\mathrm{HA}]^n} \qquad \text{Eq. 12}$$

Inserting $\mathrm{D} = \frac{[\mathrm{CdA_2(HA)_{(n-2)}}]}{[\mathrm{Cd^{2+}}]}$ and taking the logarithm of each side gives:

$$\log \mathrm{K} = \log \mathrm{D} + 2\log[\mathrm{H^+}] - \mathrm{n}\log[\mathrm{HA}] \qquad \text{Eq. 13}$$

Solving for $\log \mathrm{D}$ and introducing $\mathrm{pH} = -\log[\mathrm{H^+}]$ gives:

$$\log \mathrm{D} = 2\mathrm{pH} + \mathrm{n}\log[\mathrm{HA}] - \log \mathrm{K} \qquad \text{Eq. 14}$$

This means that when plotted as a function of pH, $\log \mathrm{D}$ should have a slope of 2. When plotted against extractant concentration, the slope should equal n, which is the number of moles of extractant that reacts with each mole of cadmium.

All isotopes of an element have approximately the same chemical properties. Therefore, when solvent extraction is performed with a feed solution containing a radioactive isotope of cadmium, the distribution ratio should equal the ratio of the radioactivity concentration in the organic phase (A_{org}) to that in the aqueous phase (A_{aq}):

$$\mathrm{D}_{Cd} = \frac{[\mathrm{Cd}]_{org}}{[\mathrm{Cd}]_{aq}} = \frac{\mathrm{A}_{org}}{\mathrm{A}_{aq}} \qquad \text{Eq. 15}$$

2.4.1 **Di-(2-ethylhexyl)phosphoric acid (HDEHP)**

Jha et al. have written a good review article on solvent extraction of cadmium from various feed solution [22]. Little or no work has been published about solvent extraction of cadmium from mixtures of nitric and phosphoric acid. Mellah and Benachour [23] demonstrated that di-(2-ethylhexyl)phosphoric acid (HDEHP) can extract cadmium from phosphoric acid. They reported that the percent extracted increased from about 10 at pH=0.5 to about 60 at pH=3.0. HDEHP is a very common extractant, and is well known in the science of solvent extraction.

2.4.2 Tri-n-butyl phosphate (TBP)

Mellah and Benachour [24] also investigated the cadmium-extraction capability of tri-n-butyl phosphate (TBP). They used analytical-grade phosphoric acid, in which they dissolved 0.5 M of Cd and added 5 mol/L of $NaNO_3$. They reported that the nitrate salt of cadmium is extractable by TBP, and that TBP extracts cadmium as a nitrate complex:

$$Cd^{2+}(aq) + 2NO_3^-(aq) + 2TBP(org) \rightleftharpoons Cd(NO_3)_2(TBP)_2(org) \quad \text{Eq. 16}$$

TBP has been used together with cation-exchanging acids in order to produce synergistic effects. In solvent extraction, a synergistic effect is when two extractants work together to produce higher distribution ratios than either of them does by itself. For example, in extraction of uranyl from 0.01 M HNO_3 into cyclohexane [20] by a the cation exchanger thenoyltrifluroacetone (TTA), TBP increased the lipophilicity of the $UO_2(TTA)_2$-complex by replacing water molecules that were associatively bonded to the coordination sites not occupied by the two TTA molecules. The increased lipophilicity led to a significant increase in the distribution ratio of uranyl. This is an example of a synergistic effect between two different extractants.

2.4.3 Trialkyl phosphine oxides (Cyanex 923)

Cyanex 923 is a mixture of four trialkyl-phosphine oxides (Table 2, page 12). Reddy et al. [25] showed that Cyanex 923 extracted cadmium from hydrochloric acid leach solutions of Ni-Cd batteries. The extracted complex was $CdCl_2 \cdot S_2$ (S=Cyanex 923). Nikam et al. found that Cyanex 923 could extract cadmium from ammonium thiocyanate medium as well [26].

2.4.4 Di-(2,4,4-trimethyl pentyl)dithiophosphinic acid (Cyanex 301)

Cyanex 301 is the trade name of di-(2,4,4-trimethyl pentyl)dithiophosphinic acid [27]. It was developed in order to recover zinc from the effluent streams of viscose plants. Zinc and calcium sulfate are present in the effluent, and it was important to selectively extract zinc.

Ocio et al. [28] found that the following reaction describes how Cyanex 301 (R_2PSSH) extracts cadmium from phosphoric acid:

$$Cd^{2+}(aq) + 2R_2PSSH(org) \rightleftharpoons Cd(R_2(P{=}S)S)_2(org) + H^+(aq) \quad \text{Eq. 17}$$

In other words, Cyanex 301 was described as a cation-exchanging extractant.

Zink and cadmium are positioned in the same group of the periodic table and therefore share many chemical properties. Selectively extracting zinc as part of the viscose process was therefore a similar challenge to that of selectively extracting cadmium as part of the Odda process. In both cases, it is important to minimize extraction of calcium. Cyanex 301 was reported by Brown et al. [29] to give 100 % extraction of zinc in the pH range 0.5-2.5, which overlaps the pH to which the mother liquor is

neutralized in the Odda process. Cyanex 301 therefore seemed like a promising extractant of cadmium in the Odda process.

However, Sole et al. [30] showed that nitric acid oxidizes Cyanex 301. They reported that contacting Cyanex 301 with HNO_3 with a concentration of more than 2 M produced fumes of nitrogen peroxide, indicating a reduction of nitric acid. Fourier-transform infrared spectroscopy of the organic phase after contact with nitric acid suggested that the sulfur atoms in Cyanex 301 had been replaced with oxygen atoms, forming di(2,4,4-trimethyl pentyl)phosphinic acid, which is sold under the trade name Cyanex 272 (Figure 6). According to the hard-soft acid base concept, the corresponding base of Cyanex 272 is a harder base than the corresponding base of Cyanex 301, because oxygen is more electronegative than sulfur. Cyanex 272 is therefore expected to extract the soft acid Cd^{2+} less effectively than Cyanex 301 does.

Sole et al. suggested that oxidation of Cyanex 301 by nitric acid also lead to the formation of disulfide-bonded dimers of Cyanex 301 (Figure 6), but they were unable to perform IR spectroscopy at a frequency low enough to observe the diagnostic stretching of the S-S-bond. Marc et al. [31] later confirmed this hypothesis by using $^{31}P\{^{1}H\}$ NMR. Mark et al. also found that the disulfides were quite stable in the presence of nitric acid. The disulfides are ineffective as extractants, so this type of oxidation also decreases the utility of Cyanex 301.

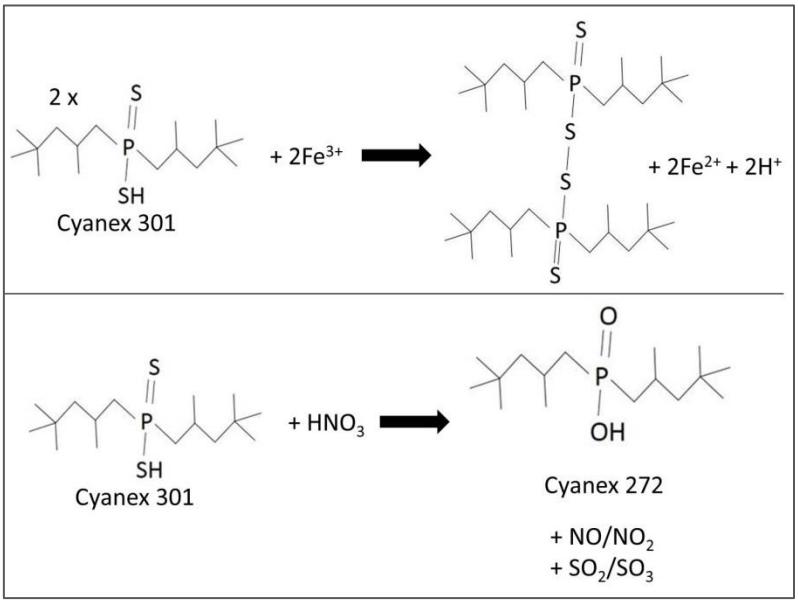

Figure 6: Cyanex 301 can be oxidized by both metal cations (top) and nitric acid (bottom).

While the oxidation of Cyanex 301 to Cyanex 272 is not reversible [32], the formation of disulfide dimer is. Perraud et al. [33] describe a method where the degenerated organic phase is contacted

with metal powder, such as zinc or nickel. In the ensuing reaction, the metal is oxidized to metal cations and the disulfides are reduced to their original monomer extractant form. The overall result is a metal-loaded organic phase, as if an undegenerated organic phase had been used to extract metal cations from an aqueous phase. The metal cations can in turn be stripped from the organic phase by contacting it with a strong acid that does not oxidize the extractant, such as sulfuric acid.

From an economical perspective, degradation could make a process based on Cyanex 301 unsustainable. However, regeneration of disulfide could extend the mean lifetime of the extractant. Moreover, it is difficult to strip from Cyanex 301 [27] and it has a nauseating smell. Overall, the literature review led to the conclusion that Cyanex 301 was an interesting extractant, although it was questionable whether it was suitable for industrial-scale extraction of cadmium from mother liquor.

3 Methods

3.1 Production of radiotracer

^{109}Cd was produced at Oslo Cyclotron Laboratory, which has a Scanditronix SC35 cyclotron capable of accelerating protons, deuterium, ^{3}He and ^{4}He. A 1 mm thick disk of natural silver was irradiated with a beam of ^{4}He-nuclei. The experiment was conducted at the same time as another experiment that used ^{4}He-nuclei with 35-MeV kinetic energy as projectiles. This other experiment used a cesium target. The portion of the beam that passed through the cesium was dumped on the silver disk. There was no means of measuring how much the cesium target attenuated the beam before it hit the silver. Therefore, the exact energy and flux of the ^{4}He-nuclei that hit the silver were unknown. However, this way of piggybacking the other experiment allowed approximately 80 hours of beam time without any cost other than that of the other experiment.

The theoretical maximum yield of ^{109}Cd was simulated. The simulated beam flux was homogeneous and monoenergetic in the entire depth of the disk, i.e. beam attenuation was ignored. Using Figure 5 as reference, the cross section for the ^{107}Ag(α,2n)^{109}In-reaction was set to 1 barn. Appendix 2 contains details on the formulas and the MATLAB-code used in the simulation.

Figure 7 shows the calculated radioactivities of ^{109}Cd and ^{109}In during radionuclide production. The time scale spans three consecutive workdays, each consisting of eight hours of irradiation, followed by 16 hours during which the beam is off. When the beam is on, the radioactivity of ^{109}In in the silver target increases rapidly, because this radionuclide has a relatively short half-life. The increase in the radioactivity of ^{109}In causes a simultaneous increase in the production rate of ^{109}Cd, because each decaying ^{109}In-nuclide turns into a ^{109}Cd-nuclide. During the 16 hours when the beam is turned off, the radioactivity of ^{109}In decays rapidly, causing a similar decrease in the growth rate of ^{109}Cd. However, ^{109}Cd is so long lived that its radioactivity grows even when the beam is off, because it has a lower decay rate than ^{109}In.

Figure 7 shows that this is a viable technique for the production of ^{109}Cd, and that under ideal conditions, one can produce more than 5 MBq of ^{109}Cd by running the cyclotron for three work days.

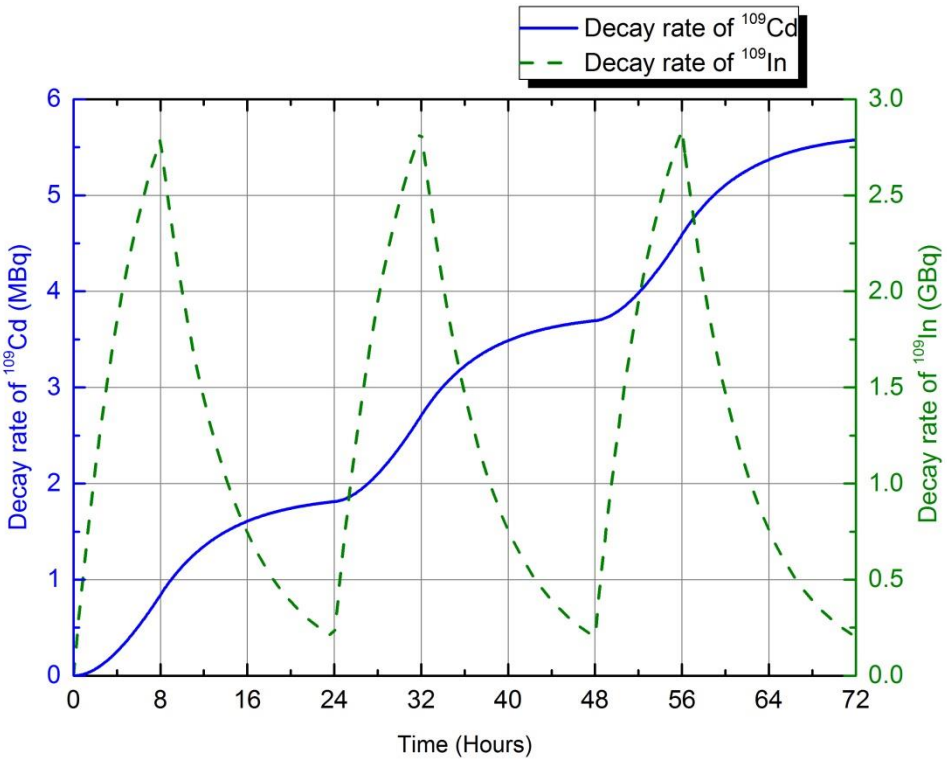

Figure 7: Calculated decay rates of ^{109}Cd and ^{109}In during radionuclide production. The target of irradiation was a 1 mm thick disk of natural silver. The projectiles were ^{4}He-nuclei. First, the disk is irradiated for 8 hours, during which the radioactivity of ^{109}In increases rapidly. Next, the beam is turned off for 16 hours, and ^{109}In decays according to its 4.2-hour half-life. All the while, the amount of the longer-lived of ^{109}Cd increases, because every ^{109}In-nuclide that decays, turns into a ^{109}Cd-nuclide.

3.1.1 Separation of ^{109}Cd from silver

For radiation-protection purposes and to avoid having to deal with the presence of three different elements in the silver disk, ^{111}In was allowed to die out before any attempts were made to separate ^{109}Cd from the silver. That was done by letting the disk sit in a shielded chamber for several weeks. After ^{111}In had died out and was no-longer visible in the γ-spectra of the silver disk (Figures 17 and 18), the cadmium was extracted from the silver disk in the following way:

The disk was cut into four pieces. The pieces where then placed in a quartz tube and heated in a tube furnace (Figure 8). During heating, a flow of helium gas passed through the quartz tube. Cadmium has a boiling point of 767 °C, while silver melts at 962 °C. Therefore, as the cadmium-bearing silver approached the boiling point of cadmium, the cadmium isotopes started to evaporate into the helium gas. The helium carried the cadmium to a gold foil placed just after the heating elements. The intention was to make the cadmium in the He gas condensate onto the gold foil. The advantage of using the gold foil was that it could be re-used after the cadmium had been washed from it. A copper coil with water passing through it was wrapped around the outside of the part of the quartz

tube where the gold foil was. A piece of quartz wool was placed inside the tube, downstream from the gold foil, as a secondary trap for cadmium.

In order to trap any cadmium which might have made it past both the gold foil and quartz wool, the helium gas was bubbled through a gas-washing bottle filled with 1.5 M HNO_3. The entire setup was placed inside a fume hood, and the exhaust from the gas-washing bottle went straight into the exhaust vent of the fume hood. The thermostat of the furnace was set to 780 °C (A thermometer inside the quartz tube showed that at its maximum, the temperature in the gas flow was 615 °C.) and the experiment was left running overnight.

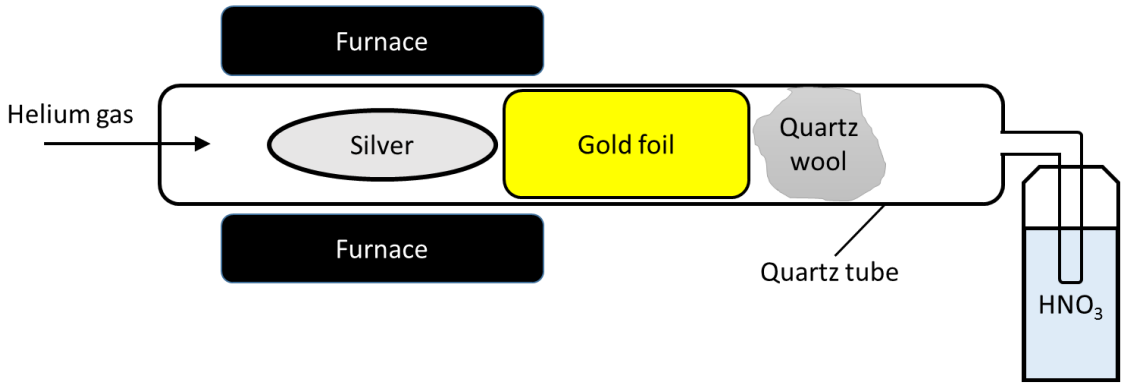

Figure 8: Sketch of how cadmium was extracted from the irradiated silver disk. Not shown in the sketch is a coil of copper tube which was wrapped around the outside of the quartz tube where the gold foil is. The entire setup was inside a fume hood.

After the furnace had been turned off, it was important to keep the gas flowing while the furnace cooled down, otherwise as the air inside the quartz tube cooled, it would contract and decrease the pressure inside the tube, thereby sucking the HNO_3 from the gas-washing bottle into the quartz tube.

Once the furnace had reached room temperature, the silver pieces, gold foil and quartz wool were taken out of the quartz tube. The inside of the tube was then rinsed repeatedly, first with 1.5 M HNO_3 and then with distilled water. The nitric acid and the water were collected in separate measuring vials. These samples, as well as the silver piece, gold foil and quartz wool were individually measured with a high-purity germanium (HPGe) detector. The HPGe-detector was also used to check for radioactivity in the HNO_3 from the gas-washing bottle. Holding a hand-held radiation monitor outside the quartz tube revealed that it still contained some radioactivity. Therefore, the quartz tube was disposed of as radioactive waste after the work had been completed.

The gold foil was washed with the same volume of acid and water that had been used to rinse out the quartz tube. This liquid became the radioactive tracer solution that was used in subsequent experiments.

The produced stock of radiotracer solution sufficed for nearly all the ensuing experiments in this project. However, in order to perform the last experiments, a few of which required a higher radioactivity concentration, 3.7 MBq of ^{109}Cd was purchased from the company Gammadata (production with the Scanditronix cyclotron was not possible at the time). The purchased tracer was delivered as 50 ml 0.1 M HCl. To avoid adding chloride to the systems under investigation, the tracer was converted to nitric acid form. The method was based on the results in Figure 24, which shows that cadmium can be extracted by 1.0 M (33 vol%) HDEHP in kerosene at pH 2, while it can be stripped back into the aqueous phase at pH=1.

Specifically, the conversion was done in the following way (Figure 9): 5 ml of the 0.1 M HCl stock solution was added to a vial. The pH in the solution was then increased to 2 by adding concentrated NH_4OH-solution. This aqueous phase was then contacted with 5 ml 1.0 M HDEHP in kerosene for ten minutes. Mixing was done with a shaking table (Figure 11). After mixing, the phases were separated by centrifuging at 2000 rpm for three minutes. Thereafter, the aqueous phase was contacted with a fresh volume of 1.0 M HDEHP, in order to extract the remaining ^{109}Cd. The volumes of organic phase from the two extraction stages were then stripped with 0.1 M HNO_3, before they were reused to extract ^{109}Cd from additional volumes of the HCl stock solution.

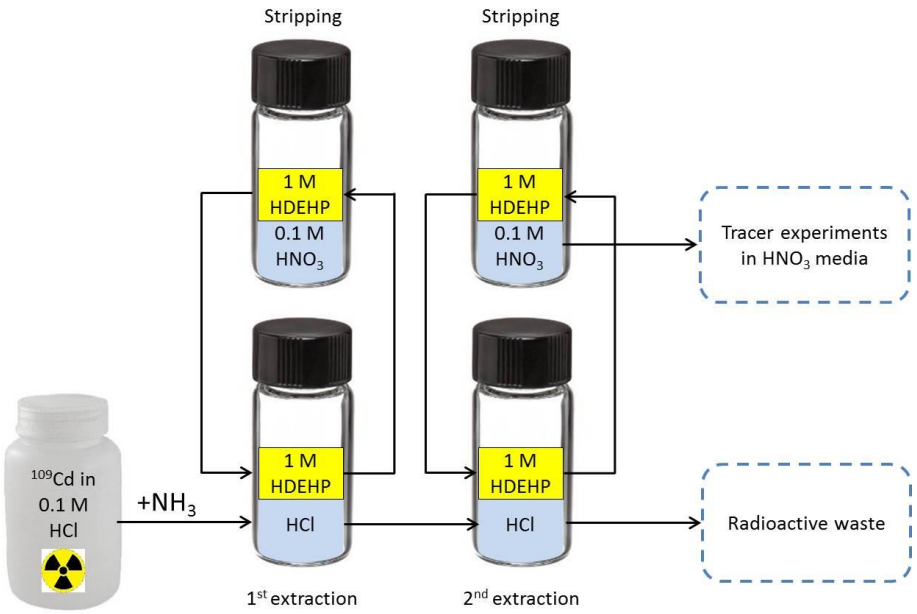

Figure 9: Schematic of the method for the conversion of the purchased radiotracer from HCl to HNO_3 form.

3.2 Analysis of mother liquor

The respective concentrations of HNO_3 and H_3PO_4 in mother liquor were determined in the following way[1]: First, 1.0 ml of the mother liquor was titrated against 0.25 M NaOH. During titration, nitric, phosphoric and hydrofluoric acid was neutralized:

$$HNO_3\ (aq) + OH^-(aq) \rightarrow NO_3^-\ (aq) + H_2O\ (l) \qquad \text{Eq. 18}$$

$$H_3PO_4\ (aq) + OH^-(aq) \rightarrow H_2PO_4^-\ (aq) + H_2O\ (l) \qquad \text{Eq. 19}$$

$$HF\ (aq) + OH^-(aq) \rightarrow F^-\ (aq) + H_2O\ (l) \qquad \text{Eq. 20}$$

To reach the equivalence point in this first titration required a volume A of NaOH. The following equation for the number of moles of acid present in the sample volume was then true:

$$N_{HNO_3} + N_{H_3PO_4} + N_{HF} = A \cdot C_{NaOH} \qquad \text{Eq. 21}$$

In this equation, N_i represents the number of moles of acid i in the sample volume and C_{NaOH} is the concentration of NaOH. After the equivalence point had been reached in the first titration (when pH began to increase rapidly, indicating that both HNO_3 and H_3PO_4 had reacted with NaOH), $H_2PO_4^-$ was converted to HNO_3 and Ag_3PO_4 by adding $AgNO_3$:

$$H_2PO_4^-\ (aq) + 3AgNO_3\ (s) \rightarrow Ag_3PO_4\ (aq) + 2HNO_3\ (aq) + NO_3^-\ (aq) \qquad \text{Eq. 22}$$

The amount of $H_2PO_4^-$ converted to HNO_3 was then determined by titration against NaOH. Calling the required volume of NaOH in this second titration B, gives the following equation for the amount of phosphoric acid present in the sample volume:

$$N_{H_3PO_4} = \frac{1}{2} \cdot B \cdot C_{NaOH} \qquad \text{Eq. 23}$$

[1] A description of the theoretical basis and the procedure for the method was provided by Tom Rames Jørgensen at Yara.

The combined amount of nitric and hydrofluoric acid can then be determined by subtracting the amount of phosphoric acid from the total amount of acid:

$$N_{HNO_3} + N_{HF} = \left(A - \frac{1}{2}B\right) C_{NaOH} \qquad \text{Eq. 24}$$

3.2.1 ICP-MS of mother liquor

Siri Simonsen at the Department of Geosciences, University of Oslo kindly performed an ICP-MS analysis of the mother liquor. The purpose of this analysis was to give an idea of the concentration of cadmium and a few other metals, which are listed along with their concentrations in Table 4 (page 39).

3.3 Radiotracer analysis of the neutralization stage

Radiotracer experiments were carried out in order to investigate how cadmium distributes between the liquid and the precipitate when mother liquor is neutralized with ammonia. Mother liquor was provided by Yara. The mother liquor was neutralized with ammonia gas in a gas-washing bottle. Figure 10 shows the setup used. Ammonia is highly hydrophilic. In order to avoid suction of mother liquor into the ammonia gas bottle, care was taken to always maintain gas pressure when the probe of the gas-washing bottle was immersed in the mother liquor. As a precaution, a water trap was installed between the gas-washing bottle and the ammonia gas bottle.

The reaction between the mother liquor and the ammonia (Eq. 3, page 6) is very exothermic. Addition of NH_3 was stopped whenever the mother liquor appeared close to boiling. Once the liquor had cooled down some, neutralization recommenced. As the pH in the liquid increased, insoluble dihydrogen phosphate salts of calcium and other metals formed and precipitated. Precipitation became pronounced as pH approached 1.5, because above this pH, the fraction of phosphate that was present as $H_2PO_4^-$ (Figure 2, page 7) became significant.

1 ml radiotracer solution was added for every 50 ml of mother liquor and the mixture was stirred for several minutes in order to allow the ^{109}Cd to distribute in the mother liquor. Then NH_3 was added using the setup in Figure 10. NH_3 was added until so much dihydrogen phosphate precipitated that the magnetic stirrer stopped turning. The solution was then centrifuged. During centrifugation, the solution separated into a precipitate and a remaining solution. The relative concentration of cadmium in the precipitate and the solution, respectively, were determined in the following way:

Two empty 20-ml scintillation vials were weighed. Next, one of the vials was filled with solution and the other with precipitate. The vials and their contents were then weighed again in order to determine the mass of sample that had been added to each. Then the radiation from ^{109}Cd in each sample was measured with gamma spectroscopy.

Because both scintillation vials were completely filled, both samples had the same counting geometry, i.e. they had the same position and orientation related to the detector during measurement. However, the precipitate was denser than the solution and could therefore potentially have a higher tendency to absorb the gamma rays from ^{109}Cd, i.e. the self-absorption could be higher in the precipitate than in the solution. To check for such a difference in self-absorption, the contents in each scintillation vial were transferred to 100-ml plastic bottles. The bottles were wider than the scintillation vials, and therefore the contents spread out more and formed thinner layers. This should reduce the effect of self-absorption because radiation from the top of each sample would have less sample material to travel through on its way to the detector which was located bellow the sample. In all cases the detector was positioned under the vial/bottle, facing upwards.

In order to investigate whether the cadmium that precipitated was bound to the crystal structure or just dissolved in water included in the precipitate, samples of the precipitate were washed with distilled water in the following way: The mass concentration of ^{109}Cd in the precipitate contained in a 20-ml scintillation vial was determined by gamma spectroscopy. Then, the precipitate was transferred to a 100-ml bottle, where it was mixed with water. Three experiments were performed, using 20, 10 and 5 ml water, respectively. After the water and the precipitate had been shaken violently for a few minutes, the mixture was centrifuged and the precipitate packed into a 20-ml vial. The relative mass concentration of ^{109}Cd was measured. The counting geometry was a little different after washing, because some of the precipitate dissolved during washing. When the amount of precipitate decreased, its center of mass shifted to a lower position in the vial, and therefore came closer to the detector, which was positioned bellow the vial as before.

Figure 10: Experimental setup for the neutralization of mother liquor by ammonia gas. The beige tube entering the picture through the left frame was connected to the gas bottle. It is connected to a water-trap which was intended to collect any liquid which might migrate against the intended direction of gas flow. To the left is the gas-washing bottle wherein the mother liquor was contacted with the ammonia. The gas-washing bottle is mounted on a magnetic stirrer. The tube leaving through the right frame of picture leads any effluent gas directly to the fume-hood exhaust vent. In the center of the picture is a bottle used for holding the head of the gas-washing bottle whenever the gas flow was not on.

3.4 Solvent extraction

Each solvent extraction experiment was carried out in the following way: 5 ml of acid was added to a 20-ml scintillation vial. Then 200 μl of tracer solution was added and the solution was mixed before 5.2 ml of organic phase was added. In later experiments, when the stock of tracer solution started to diminish, the amount of tracer added was reduced to 100 μL and the organic phase reduced to 5.1 in order to maintain a phase ratio of 1. The tracer solution consisted of 0.8 M HNO_3.

In the initial experiments, the phases were mixed by using a magnetic stirrer at 1250 rpm for 5 minutes. In order to be able to run more experiments simultaneously, a shaking table was used in later experiments (Figure 11). The shaking table made it possible to perform the mixing stage of ten experiments at the same time, under identical shaking speeds and times.

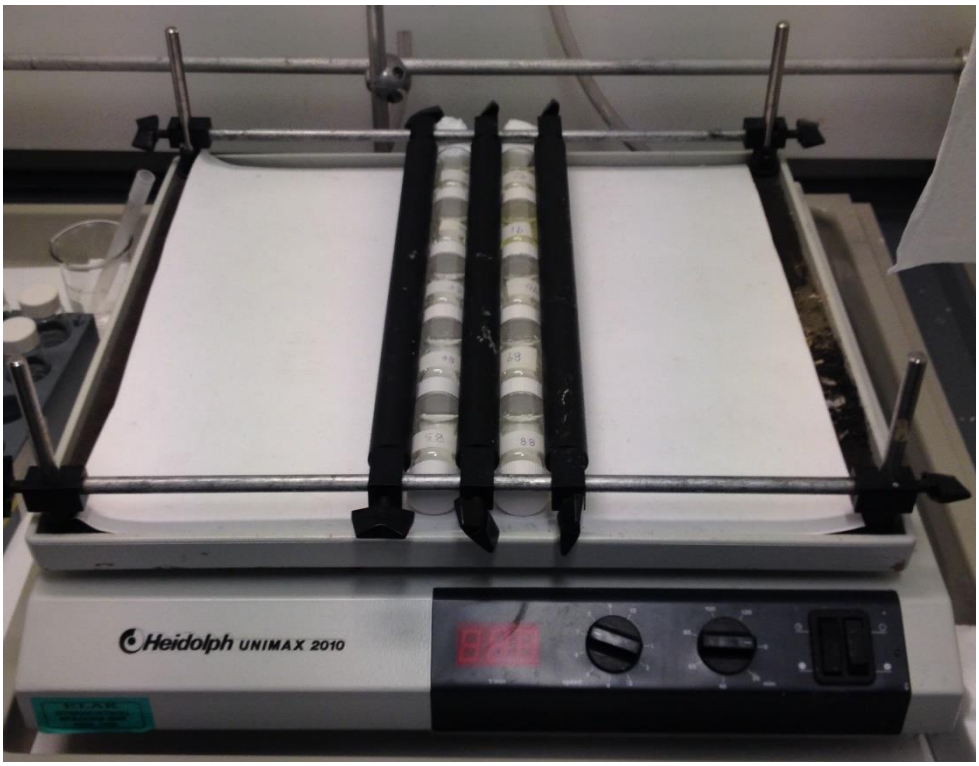

Figure 11: Shaking table with ten liquid scintillation vials ready for performing the mixing stage of the solvent extraction experiments.

After mixing, the solution was transferred to a centrifuge vial and the phases were separated by centrifuging at 2000 rpm for 3 minutes. The heavier aqueous phase went to the bottom of the centrifuge vial. After centrifuging, 3.5 ml of the organic phase was transferred to an LSC vial containing 10 ml LSC-cocktail. The remaining organic phase was disposed of as radioactive waste. In order to remove any residual organic phase on the top of the aqueous phase, the top 0.5 ml of aqueous phase was disposed of as radioactive waste. Finally, 3.5 ml aqueous phase was sucked up from the bottom of the vial and transferred to an LSC vial containing 10 ml of LSC cocktail. The remaining aqueous phase was disposed of as radioactive waste.

The volume of each phase transferred to LSC-vials for counting was in the initial experiments only 1.0 ml, but this volume was gradually increased to 3.5 ml in order to increase the count rates and thereby reduce the required counting times. The change in sampled volume did not appear to have any negative effect on counting efficiency.

The abilities of the extractants HDEHP, Cyanex 301, Cyanex 272, Cyanex 923 and TBP to extract Cd from a mixture of HNO_3 and H_3PO_4 were investigated at different pH-values. pH was adjusted by diluting the acid solution to three different concentrations: 0.5 M, 0.05 M and 0.005 M nitric and phosphoric acid, and then adding tracer. The resulting concentration of nitric acid depended on how

much tracer solution was added, because the tracer solution consisted of 0.8 M HNO_3. Cyanex 301 and HDEHP were also tested at pH=2, which was obtained by neutralizing 0.005 M HNO_3 and H_3PO_4 with concentrated NH_4OH after tracer had been added. The organic phases consisted of 0.2 M extractant in kerosene. Kerosene was elected as the organic diluent in all the experiments in this work because it is widely used in industry.

In order to verify that equilibrium was achieved during the extraction experiments, the stirring and shaking times were varied.

In order to try to increase the distribution ratios found with 0.2 M HDEHP in the screening, the experiments were repeated with 1.0 M HDEHP. 1.0 M is close to the highest possible concentration of HDEHP one can achieve in kerosene and still have a homogeneous mixture. At higher concentrations, one can see with the naked eye that the mixture becomes heterogeneous.

The effects of changing extractant concentration were investigated for both HDEHP and Cyanex 301. This was done by performing a series of experiments with varying extractant concentrations and a constant aqueous phase.

The results obtained with 1.0 M HDEHP (Chapter 4.4) suggested that it might be suitable for extraction of cadmium from mother liquor. Extraction from mother liquor was more challenging than extraction from "synthetic" (i.e. laboratory prepared) nitric and phosphoric acid solutions. First, the mother liquor was neutralized to approximately pH=1.5, using NH_3 gas. Then concentrated NH_4OH-solution was added to increase the pH to 2. Thereafter, aqueous solution was contacted with 1.0 M HDEHP. During mixing, the pH in the aqueous phase decreased to 1.6. This is probably due to the protons released from HDEHP during the reaction with cations (Eq. 11, page 13). The mother liquor contains high concentrations of metal cations (Table 4, page 39), while the previous experiments dealt with mixtures of pure nitric and phosphoric acid containing only tracer concentrations of cadmium, and no other metal cations. With only tracer concentrations, the acidic effect of HDEHP was assumed to be negligible, and pH was therefore only measured before mixing with organic phase, not after.

During extraction from mother liquor, on the other hand, the acidic effect of HDEHP became significant. In order to counteract this effect, the pH was measured after the phases had been separated. Then concentrated NH_4OH-solution was added until the pH was above 2. Then the two phases were mixed and centrifuged again. This was repeated until the pH in the aqueous solution was 2.3 after separation.

3.5 Measurement of radioactivity

Liquid scintillation counting (LSC) is a technique for the detection and quantitative measurement of radioactivity. It gives high detection efficiencies for radionuclides which emit charged particles such as α-particles and electrons. To measure the radioactivity content in a solution, a sample of the solution is mixed with a scintillation cocktail consisting of an organic solvent, a surfactant and a fluorescent compound [15]. When a charged particle such as a conversion electron travels through the LSC-cocktail, it transfers its kinetic energy to the organic solvent molecules around it by exciting them. This energy then continues from the solvent molecules to the fluorescent molecules, which convert the energy to pulses of visible light. The sample is contained in a transparent vial. Outside the vial are photomultiplier tubes (PMTs), which are electronic devices that are able to measure the number of photons in each pulse (the pulse height). The number of photons correlates with the energy deposited in the cocktail by the charged particle.

The output from an LSC-measurement is a histogram of the observed light pulses. Such histograms are called spectra (Figure 12). Along the first axis of a spectrum are the channel numbers. Each channel represents an interval on the scale of light pulses. Higher channel numbers represent higher pulses, and higher pulses correspond to higher-energy radiation. Along the second axis is the number of observations of light pulses falling within each channel. This is where the technique gets its name from; it counts the scintillation events in a liquid.

The term “count rate” describes the number of decay events a radioactivity detector observes per unit time. It is often reported as counts per second. The decay rate is the actual rate of disintegration within the sample, reported in units of decays per second, which in the SI-system is called Becquerel (Bq). The counting efficiency of a detector is the ratio of the count rate to the decay rate. LSC often provides good counting efficiencies compared to other techniques. However, determining the counting efficiency is not always straightforward due to an effect termed "quenching".

The term “quenching” describes any decrease in the transport of energy from the ionizing radiation via the scintillation cocktail to the PMTs. The most common causes for quenching are chemical quenching and color quenching. Chemical quenching occurs when the cocktail contains a chemical that can absorb the energy of the emitted radiation before it results in light emission. Color quench occurs when the sample contains colored species, which absorb some of the photons emitted by the scintillating agent. Both chemical and color quenching reduce the count rate and the observed height of the light pulses. Therefore, quenching causes a correlated decrease in counting efficiency and a shift of the spectra to lower channels.

Figure 12 shows the liquid scintillation spectrum of the ^{109}Cd radiotracer that was produced. The spectrum contains three peaks. The two lower peaks are due to Auger electrons [34]. The leftmost peak is due to Auger electrons from the L- and higher shells. The middle peak is due to Auger electrons from the K-shell. The third and most intense peak is due to conversion electrons. The spectrum measured in this work, with a HIDEX 300 SL instrument, matches the spectrum from Kossert et al. [34] and gives confidence that our tracer is not contaminated with other radionuclides from unwanted reaction channels during production.

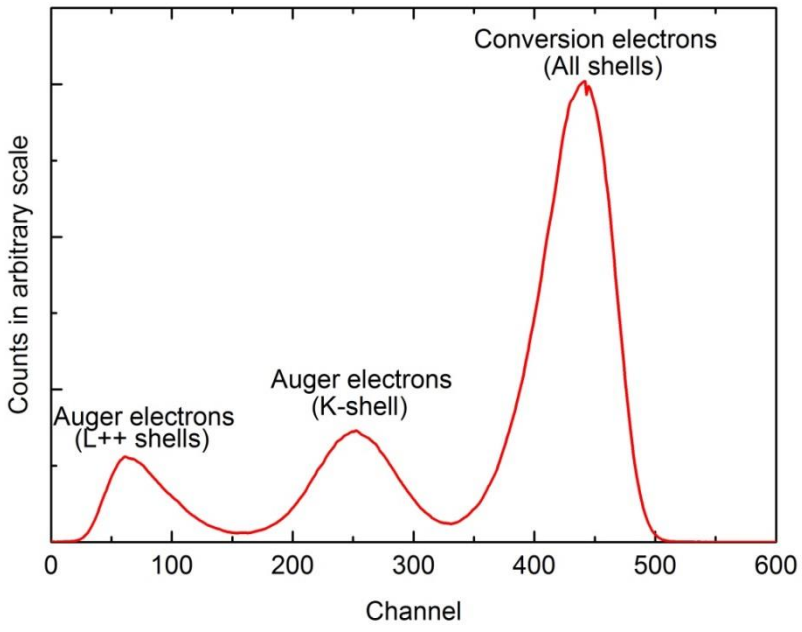

Figure 12: Liquid-scintillation spectrum of the produced tracer solution. Based on Kossert et al.[34].

3.5.1 Quench correction

In order to correct for quenching, three parallel samples were prepared in the following way: 10 ml scintillation cocktail was added to an LSC-vial. Then, 50 μL of tracer solution was added before the vial was capped and shaken violently by hand for two minutes. Then, an LSC-spectrum was taken. Then, 50 μL of filtered mother liquor was added, the vial shaken violently by hand for two minutes and another spectrum taken. Several more spectra were measured, and before each measurement, more mother liquor was added to the sample. The count time was the same for each measurement. The quenching analysis was performed for two different brands of liquid scintillation cocktail, Gold Star and Instagel Plus, respectively, because we ran out of Gold Star after a few experiments.

Figure 13 shows how the LSC-spectrum from one of the parallels using Gold Star changed as the mother-liquor content in the sample increased. One can clearly see that the maximum of the highest

peak of the spectrum shifted to progressively lower channels. The height of the maximum decreased as well. This was expected from the theory for quenching. More quenching makes the light pulses weaker, which causes the peaks in the spectrum to shift to lower channels. More quenching also makes the peaks wider. Quenching also make some pulses so weak that the PMTs do not detect them. Quenching therefore decrease the count rate. The effect of quenching on the leftmost peak was less regular than it was on the rightmost peak. The height of the leftmost peak did not consistently decrease as the mother liquor content increased. For example, this peak was highest when the sample contained 250 μL mother liquor.

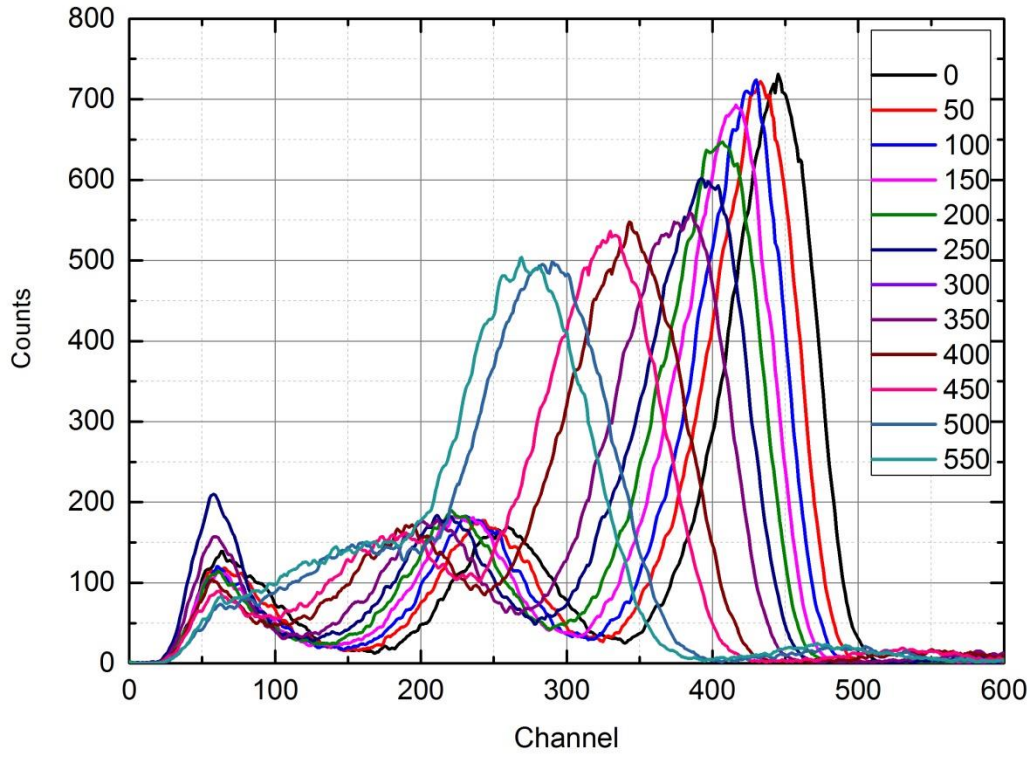

Figure 13: The liquid scintillation counting spectra of a sample containing 100 μl tracer solution in 10 ml LSC-cocktail, as well as the indicated amount of mother liquor (in μl). Notice the shift to lower channels as the amount of mother liquor increased.

The shift of the peaks to lower channels was used to create a calibration function for quenching. A computer program was written to find the channel of the maximum of the highest peak, as well as to calculate the number of counts. The number of counts was calculated by summing the counts in all the channels defined by a Region of Interest (ROI). The relative counting efficiency for a given spectrum was defined as the number of counts observed divided by the number of counts in the least quenched spectrum. Another computer program was designed to calculate the ROI which gave the best linearity between the channel of the maximum of the highest peak and the relative counting efficiency. The goodness of fit was evaluated by calculating R^2 for the relative efficiency as a function

of the channel of the maximum of the highest peak. All computer programs were written in MATLAB. Appendix 4 contains the scripts for the computer programs.

For Gold Star, if the leftmost peak was included in the ROI there was poor correlation between the channel of the maximum of the highest peak and the relative efficiency (Figure 14). This was probably because of the irregularities in how quenching affected the lowest peak.

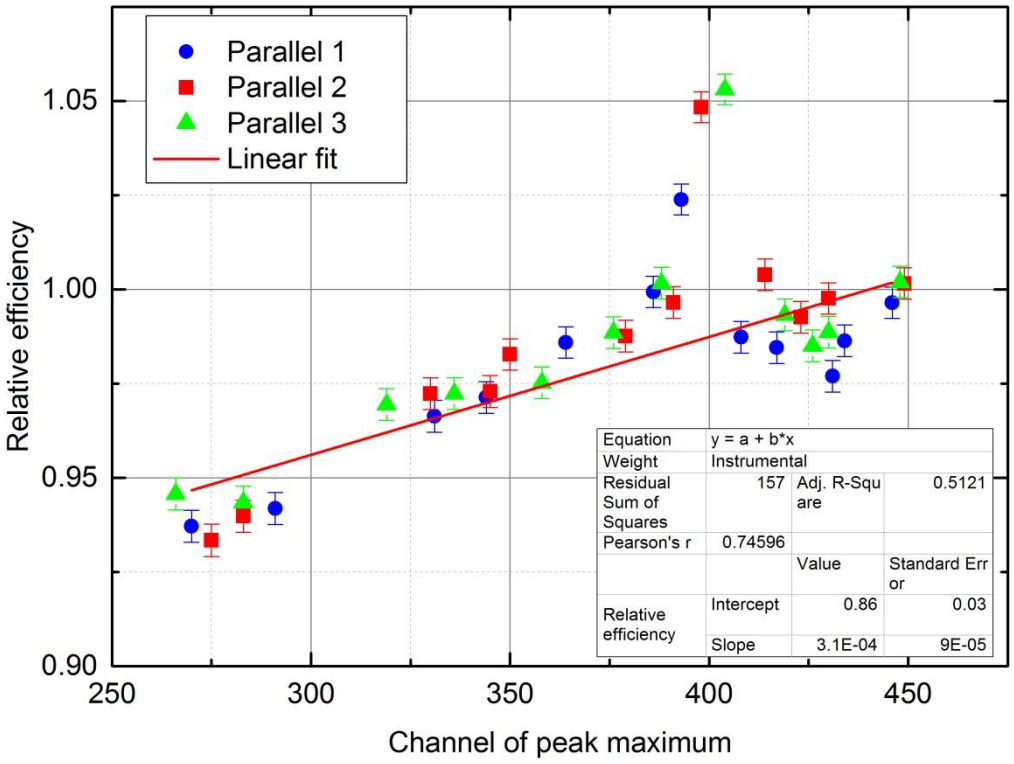

Figure 14: Calibration plot using the liquid scintillation cocktail Gold Star, using a region of interest which extends from 0 to 1023.

Using the optimal ROI which the computer program calculated gave the calibration plot in Figure 15, which is a plot with much better correlation between the fitted line and the calculated relative efficiencies. The optimal ROI was found to extend from channel 191 to channel1023, i.e. it does not include the lowest peak. The fitted line in Figure 15 was used to calculate the relative efficiency in subsequent measurements using Gold Star.

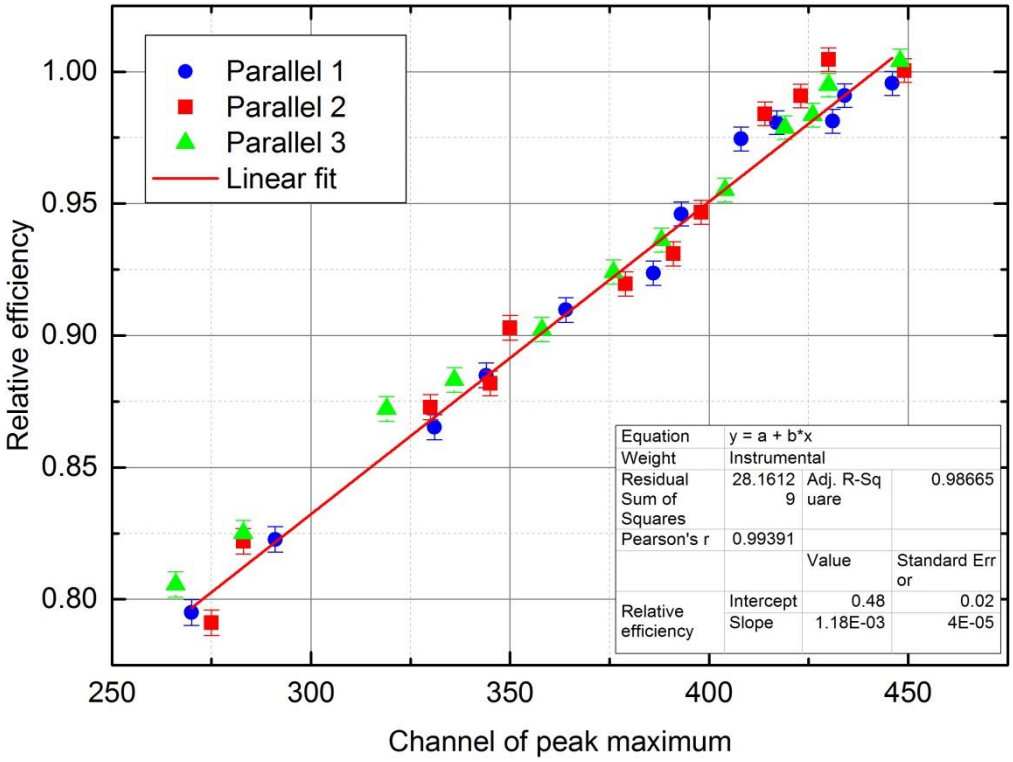

Figure 15: Calibration plot using the liquid scintillation cocktail Gold Star, using the optimal region of interest for Gold Star, which is from channel 191 to channel 1023.

With the LSC cocktail Instagel Plus, the optimal ROI was found to extend form channel 41 to channel 1023, but the difference in linear correlation between the optimal ROI and the one that extended from 0 to 1023 was considered negligible, so for simplicity the ROI was set to extend from 0 to 1023 in future measurements. Figure 16 shows the calibration plot for Instagel Plus.

The following equation was used to calculate the relative efficiency E from the channel of the maximum of the highest peak, x:

$$E = a \cdot x + b \qquad \text{Eq. 25}$$

a is the slope of the calibration plot and and b is the intercept. An expression for the uncertainty in E was derived in the following way:

$$\sigma_E = \sqrt{\left(\frac{\partial E}{\partial a}\sigma_a\right)^2 + \left(\frac{\partial E}{\partial b}\sigma_b\right)^2} \qquad \text{Eq. 26}$$

σ_a and σ_b are the standard errors of a and b, respectively. Calculating $\frac{\partial E}{\partial a} = x$ and $\frac{\partial E}{\partial b} = 1$ and inserting these in Eq. 26, give the following expression for σ_E:

$$\sigma_E = \sqrt{(x\sigma_a)^2 + \sigma_b^2} \qquad \text{Eq. 27}$$

Table 3 lists the coefficients a and b, as well as their standard errors for both Gold Star and Instagel Plus.

Table 3: The coefficients of the calibration functions for the two LSC-cocktails Gold Star and Instagel Plus. a is the slope of the line and b is the intercept. σ_a is the standard error of a and σ_b is the standard error of b.

Cocktail	a	σ_a	b	σ_b
Gold Star	$1.18 \cdot 10^{-3}$	$4 \cdot 10^{-5}$	0.48	0.02
Instagel Plus	$6.7 \cdot 10^{-4}$	$4 \cdot 10^{-5}$	0.70	0.01

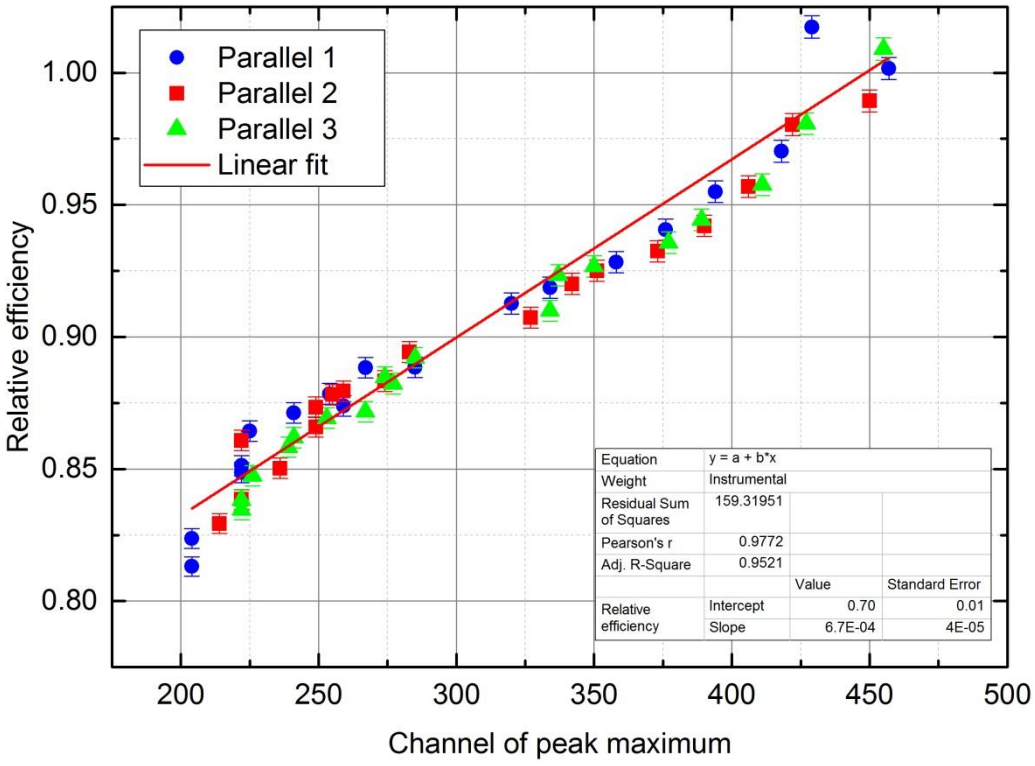

Figure 16: Calibration plot using the liquid scintillation cocktail Instagel Plus. The region of interest was set to extend from 0 to 1023.

The distribution ratio in a solvent extraction experiment was measured in the following way. An LSC spectrum was obtained. Then the number of counts in the ROI was calculated by summarizing the number of counts in each channel within the ROI. Then the number of counts in the ROI was divided by the count time in order to calculate the count rate. Then the channel where the maximum of the highest peak occurred was used to calculate the relative counting efficiency. Then the count rate was divided by the relative counting efficiency to give an efficiency-corrected count rate. The distribution

ratio was then calculated by dividing the efficiency-corrected count rate of the organic phase by the efficiency-corrected count rate of the aqueous phase, given that the sample volumes for each phase had been equal. Appendix 3 contains more details on how the radioactivity was measured, as well as uncertainty calculations.

The quality of the LSC-based method was controlled by measuring two distribution ratios both with LSC and gamma spectroscopy. This was done by performing two parallels of an extraction experiment and transferring identical volumes of each phase to separate and identical vials. The amount of ^{109}Cd in each vial was then measured by gamma spectroscopy, with identical counting geometry. Ignoring self-absorption, which is negligible for dilute solvents, the distribution ratio of cadmium should equal the count rate from the organic phase divided by the count rate from the aqueous phase. After the distribution ratio had been measured with gamma spectroscopy, it was measured with the LSC-based method, and the two distribution ratios were compared.

4 Results and discussion

4.1 Production of radiotracer

Figure 17 shows a γ-spectrum of the silver disk taken a few days after it was removed from the target chamber where it had been irradiated. The presence of ^{111}In is evident by its 171.3 and 245.4-keV γ-emission lines (See Table 1, page 11 for a list of relevant γ-energies and intensities). The 88-keV γ-line of ^{109}Cd is much weaker, but visible. The 203.5-keV line of ^{109}In is not observed, which indicates that as expected, practically all ^{109}In-nuclide had decayed to ^{109}Cd after just a few days.

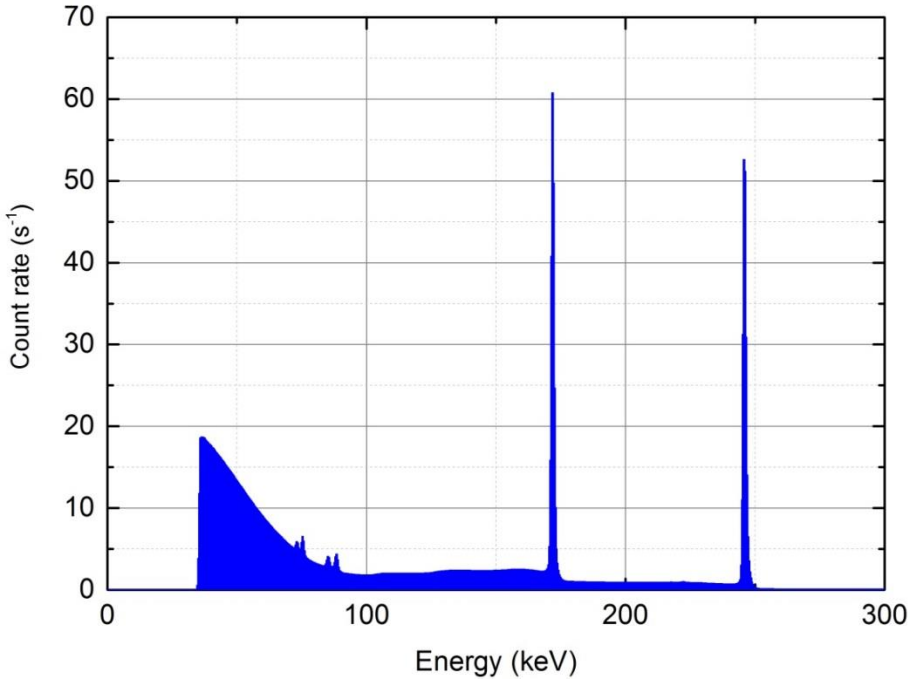

Figure 17: γ-spectrum of the irradiated silver disk a few days after irradiation. The 171.3 and 245.4-keV γ-emission lines of ^{111}In are clearly shown. The 88-keV peak of ^{109}Cd is also visible.

Figure 18 shows a γ-spectrum of the silver disk taken 29 days later than the spectrum in Figure 17. As expected due to its half-life of 2.8 days, the presence of ^{111}In had at decreased approximately 1000-fold in that time. At this point, ^{109}Cd was the only radionuclide in the sample and the work to separate cadmium from silver could commence.

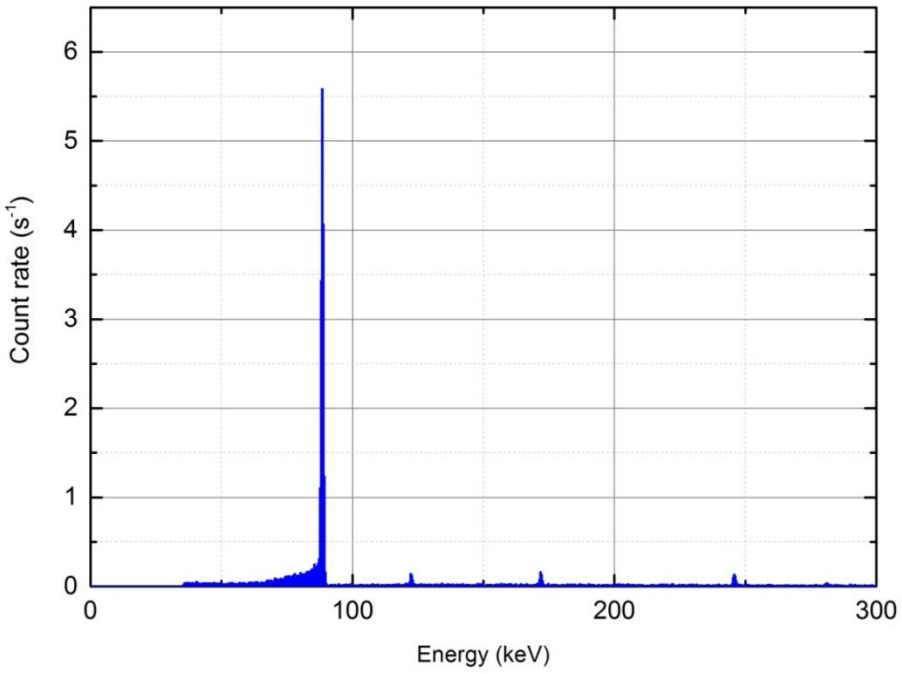

Figure 18: Gamma-spectrum of the silver disk taken 29 days after the one shown in Figure 17. Comparison with Figure 17 shows that 111In has diminished greatly due to radioactive decay, making it easier to distinguish the 88-keV peak of the longer-liver 109Cd (Beware of the different scales of the y-axes in the two spectra).

The method to separate cadmium from the silver disk worked. LSC-analysis showed that the tracer solution had a radioactivity concentration of at least 2 kBq/ml. The radioactivity concentration can be converted to molar concentration in the following way:

The number N of ^{109}Cd-nuclides per milliliter is given by the radioactivity concentration $\mathrm{R} = 2 \cdot 10^3\ \mathrm{Bq/ml}$, divided by the decay constant $\lambda = \frac{\ln 2}{T_{1/2}} = 2 \cdot 10^{-8}$, where $T_{1/2}$ is the half-life of ^{109}Cd in seconds:

$$\mathrm{N} = \frac{\mathrm{R}}{\lambda} = \frac{2 \cdot 10^3\ \mathrm{Bq/ml}}{2 \cdot 10^{-8}\ \mathrm{s^{-1}}} = 1 \cdot 10^{11}\mathrm{ml^{-1}} \qquad \text{Eq. 28}$$

Dividing by the Avogadro constant gives the number of moles of ^{109}Cd in 1 ml. Multiplying by 1000 gives the concentration in molar:

$$\left[^{109}\mathrm{Cd}\right] = \frac{1 \cdot 10^{11}\ \mathrm{ml^{-1}}}{6.02 \cdot 10^{23}\ \mathrm{mol^{-1}}} \cdot 1000\ \mathrm{ml/l} = 2 \cdot 10^{-10}\ \mathrm{M} \qquad \text{Eq. 29}$$

Therefore, the concentration of cadmium in the tracer solution is very low, and hardly detectable with non-radiochemical techniques.

A total volume of approximately 50 ml of the tracer solution was produced, and the produced tracer solution was usable for extraction experiments. Therefore, the goal of producing a radioactive Cd-tracer was achieved.

However, the radioactivity concentration of the tracer solution should ideally have been higher. A first step towards increasing the radioactivity concentration would have been to improve the process of separating Cd from the silver disk, because it would reduce the volume of acid and water used to rinse out the quartz tube and gold foil. Doing so would probably include optimizing the He-gas flow, furnace temperature and perhaps most importantly finding a replacement for the gold foil, i.e. a surface on which the Cd in the He-gas could efficiently condense and later be washed of by dilute acid.

Alternative methods for the separation of Cd from Ag include wet separation techniques in which the silver disk is dissolved entirely, and then separation is carried out through a chemical process. For example, one may dissolve the silver disk in concentrated nitric acid and then add hydrochloric acid in order to precipitate and filter of AgCl. Excess hydrochloric acid could in turn be evaporated and one should in theory be left with only Cd in solution. However, with Cd being present in only tracer amounts, there is a risk of co-precipitation of Cd in AgCl, and it is inevitable that some Ag remains in solution. Other viable chemical separation techniques include using ion exchange resins or solvent extraction, but using those techniques would require reagents that would be very selective towards either Ag or Cd. Following chemical separation, one should ideally recycle the silver i.e. by electroplating it. By comparison, dry distillation seemed like a more straightforward and less messy approach. However, from a radiation protection perspective, the potential hazards are usually greater when working with radioactivity in gas phase rather than in solutions, due to the risk of inhaling the radioactivity, which is more severe than getting a radioactive solution on the skin.

4.2 Analysis of mother liquor

Figure 19 is a plot of the pH as a function of added volume of 0.25 M NaOH during the first titration stage. It shows that the equivalence point was reached after (29 ± 1) ml NaOH. Inserting this for A in Eq. 21 (page 22) gives a total acid content of (7.3 ± 0.3) mmol in the 1 ml sample volume, giving a total acid concentration of (7.3 ± 0.3) M in the mother liquor. In the first titration stage, addition of NaOH was halted when the pH began increasing rapidly. The result from the first titration could have been more accurate if more NaOH had been added, so that the equivalence point would have become more clearly visible in the plot. However, care was taken in order to not add too much NaOH, because that would affect the second titration stage. To compensate for the early cut-off in Figure 19, a fairly large uncertainty of 1 ml was used in the calculations based on the observations.

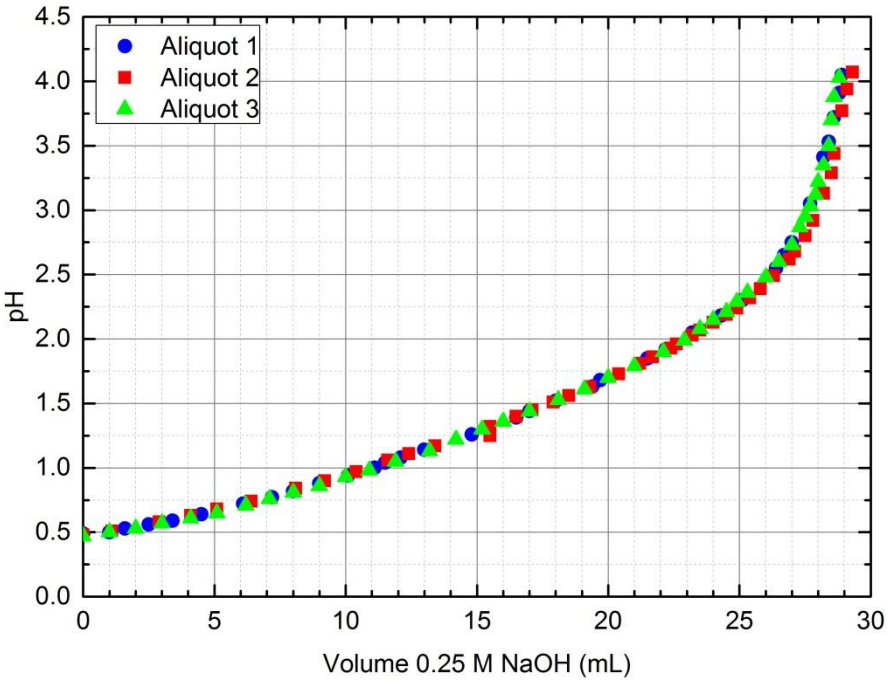

Figure 19: pH as a function of added volume of 0.25 NaOH during the first titration stage of the analysis of the mother liquor.

Figure 20 is a plot of the second titration stage. In this stage, the equivalence point is reached after (31 $\pm$ 1) ml of NaOH. Inserting this for B in Eq. 23 (page 22) gives a phosphoric acid concentration of (3.9 $\pm$ 0.1) M. Subtracting the phosphoric acid concentration from the total acid concentration gives a combined concentration of nitric and hydrofluoric acid of (7.3 $\pm$ 0.3) M - (3.9 $\pm$ 0.1) M = (3.4 $\pm$ 0.3) M.

Eq. 1 (page 5) shows that it takes ten moles of HNO_3 in order to produce three moles of H_3PO_4 by dissolution of apatite in nitric acid. To produce (3.9$\pm$ 0.1) M H_3PO_4 would therefore require 10/3 $\cdot$ (3.9$\pm$ 0.1) M = (13.0 $\pm$ 0.3) M HNO_3. Ignoring the water and hydrofluoric acid lost to evaporation during dissolution, a combined concentration of residual HNO_3 and HF of 3.4 M suggests that the initial concentration of the nitric acid used to acidulate apatite was 13 M + 3.4 M = 16.4 M. This is equivalent to 73 vol% HNO_3. According to Tom Jørgensen at Yara, they use 58 vol% HNO_3. The difference can be explained by evaporation of water due to the heat of reaction during dissolution of the phosphate rock. The acid concentration increases when water evaporates. This shows that the results are reasonable.

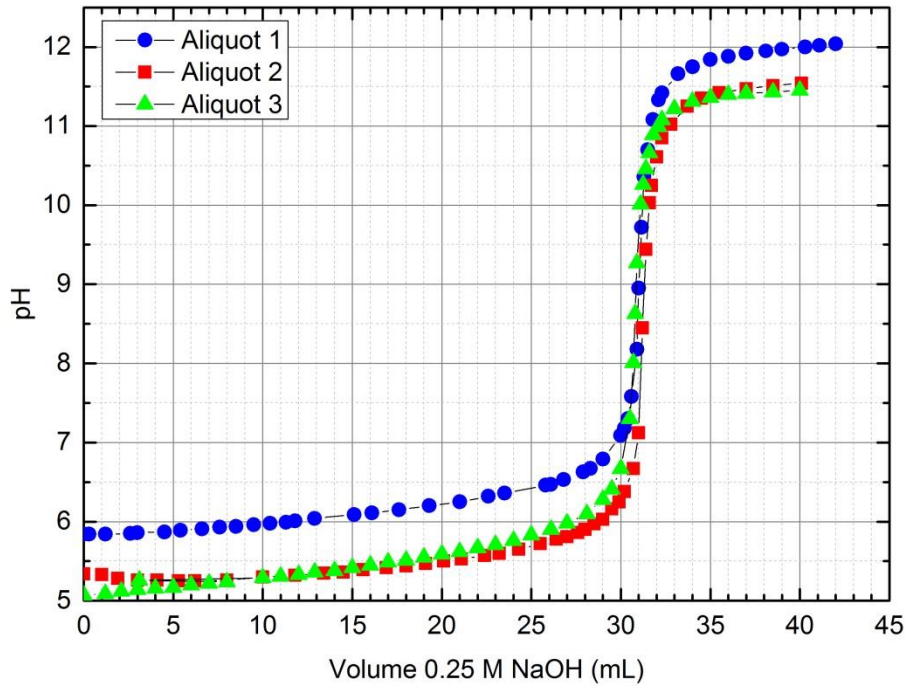

Figure 20: pH as a function of added volume of 0.25 M NaOH during the second titration stage of the analysis of the mother liquor.

Table 4 shows the result of the ICP-MS-analysis of the mother liquor. It shows that cadmium, lead, rubidium and strontium are present in the parts-per-million-range. There is significantly more barium, magnesium, vanadium, chromium, manganese, iron, nickel, copper and zinc present.

Table 4: Concentrations of selected metals in the mother liquor, measured by ICP-MS. The concentrations of Rb and Sr are semi quantitative and probably too low, because standards for Rb and Sr were not measured. When converting from mass concentration to molar concentration, it is important to keep in mind that the density of the mother liquor is 1.47 kg/l.

Element	Mass concentration	Concentration (M)	Element	Mass concentration	Concentration (M)
Cd	(9.2 ± 0.1) ppm	$1.20 \cdot 10^{-4} \pm 2 \cdot 10^{-6}$	Fe	(83 ± 1) ‰	2.17 ± 0.02
Ba	(1.8 ± 0.1) ‰	$1.94 \cdot 10^{-2} \pm 7 \cdot 10^{-4}$	Co	(0.23 ± 0.08) ppm	$6 \cdot 10^{-6} \pm 2 \cdot 10^{-6}$
Pb	(2.9 ± 0.4) ppm	$2.1 \cdot 10^{-5} \pm 3 \cdot 10^{-6}$	Ni	(89 ± 1) ppm	$2.24 \cdot 10^{-3} \pm 4 \cdot 10^{-5}$
Mg	(2.46 ± 0.03) ‰	0.149 ± 0.002	Cu	(73.4 ± 0.7) ppm	$1.70 \cdot 10^{-3} \pm 2 \cdot 10^{-5}$
V	(187 ± 6) ppm	$5.4 \cdot 10^{-3} \pm 2 \cdot 10^{-4}$	Zn	(0.49 ± 0.01) ‰	$1.10 \cdot 10^{-2} \pm 2 \cdot 10^{-4}$
Cr	(1.9 ± 0.1) ‰	0.053 ± 0.003	Rb	1* ppm	$2 \cdot 10^{-5}$
Mn	(58 ± 1) ppm	$1.56 \cdot 10^{-3} \pm 2 \cdot 10^{-5}$	Sr	5* ppm	$8 \cdot 10^{-2}$

4.3 Radiotracer analysis of the neutralization stage

Three experiments were performed in order to investigate how cadmium distributes between the precipitate and the solution when mother liquor is neutralized with ammonia gas. Ammonia gas was added until so much precipitate formed that the solution turned to a crud that inhibited further addition of ammonia. Then the solution and precipitate were separated by centrifuging. The pH in the solution after neutralization was 1.1, 1.2 and 1.5 in the respective experiments. Approximately half of the initial volume of the solution was left after centrifugation. The other half had precipitated. The temperature at the time of centrifuging was not controlled.

The count rate from ^{109}Cd per unit mass was assumed to be proportional to the mass concentration of cadmium in each phase. As described in section 3.3, the radioactivity concentration in the wet precipitate and the solution were measured with gamma spectroscopy. The results showed that in all of the three experiments, there was a 1:1 ratio between the cadmium concentration in the wet precipitate and in the remaining solution. The precipitate was not dried before weighing and gamma spectroscopy, because drying would not change the amount of cadmium contained in the precipitate.

Table 5 shows the results from the experiment which was aimed at correcting for the potential difference between self-absorption in the precipitate and in the remaining solution. It shows that there is no significant increase in count rate when either of the samples is distributed onto a wider surface. The small increase observed for the precipitate is almost equal to the standard deviation of the count rate observed when the sample was in a 100-ml bottle and can therefore be disregarded. Therefore, self-absorption is not large enough to force a correction of the observations in the above results.

Table 5: Decay-corrected count rate from ^{109}Cd per unit mass for the precipitate and remaining solution from when mother liquor is neutralized with ammonia. Observations made from one parallel.

	Solution	Precipitate
Count rate when in 20-ml vial ($s^{-1}g^{1}$)	0.110 ± 0.004	0.105 ± 0.003
Count rate when in 100-ml bottle ($s^{-1}g^{1}$)	0.110 ± 0.004	0.12 ± 0.01

Table 6 shows the observations made when washing the precipitate with distilled water. It shows that washing increased the Cd concentration in the precipitate. This could mean that when the precipitate forms during neutralization of mother liquor by NH_3, Cd is incorporated into the crystal structure. When the precipitate is washed, some of the more soluble metal salts dissolve, while cadmium has a greater affinity for the precipitate. Therefore the Cd concentration in the remaining

precipitate increases. If the count rate per mass had decreased as a result of washing, it could have indicated that the radioactive tracer was mostly present in the water included in the precipitate, and not bonded to the precipitate itself. Washing with water would then replace the radioactive water in the precipitate with non-radioactive water, and decrease the count rate per mass. The results show that this is not the case, and that cadmium binds to the precipitate.

Ideally, smaller volumes of water should have been used in these experiments, because so much precipitate dissolved during washing that the counting geometry for gamma spectroscopy changed, which may have led to artificially high count rates after washing. This source of error could have been counteracted by moving the sample further away from the detector. However, that would have gone on the account of count rates, and peak-to-background-ratios, and was therefore not done. This dilema could have been avoided by using a higher radioactivitiy concentration.

Table 6: The results of washing the precipitate formed during neutralization of mother liquor with water.

Experiment number	Mass before washing (g)	Volume of water used to wash (ml)	Count rate per mass before washing (cps/g)	Mass after washing (g)	Count rate per mass after washing (cps/g)
1	33	20	0.102 ± 0.001	5	0.18 ± 0.02
2	34	5	0.091 ± 0.001	16	0.122 ± 0.004
3	33	10	0.103 ± 0.001	8	0.120 ± 0.008

4.4 Solvent extraction of cadmium

4.4.1 Quality control of the method

The results of the solvent extraction experiments are presented in this section. Each experiment was performed twice. In each plot, uncertainties are presented as error bars. The error bar in each data point represents the larger of the propagated error from the detector uncertainty and the standard deviation of the results from the two parallels that were performed in each experiment. Equal volumes of each phase were used in all experiments. Cadmium was present in tracer concentration in every experiment.

Table 7 shows the distribution ratios observed in two parallels of the same solvent extraction experiment. The distribution ratio in each parallel was measured both with LSC and gamma spectroscopy. For the first parallel, the two methods yielded results that were within four standard deviations of each other. The difference could be due to random errors, such as inaccurate pipetting.

If the volumes of the samples of the respective phases differed, either the volume measured with gamma spectroscopy or the volume measured with LSC, the interpretation of the measurements would yield different distribution ratios. For the second parallel, the difference is less than one standard deviation. Most importantly, both gamma spectroscopy and LSC yielded the same average distribution ratio and standard deviation for the two parallels. This indicates that the method developed for measuring distribution ratios with LSC is accurate. Ideally, and given time, a few more experiments wherein LSC and gamma spectroscopy were compared should have been performed. However, the results described in the following text were obtained with the LSC method and they correspond well with theory. That indicates that the LSC method is accurate.

Table 7: Comparison of the results obtained by measuring the distribution ratio of cadmium by both liquid scintillation counting (LSC) and gamma spectroscopy.

	Distribution ratio measured with LSC	Distribution ratio measured with gamma spectroscopy
Parallel 1	0.95 ± 0.03	1.06 ± 0.01
Parallel 2	1.40 ± 0.04	1.43 ± 0.02
Average $\pm$ standard deviation	1.2 ± 0.3	1.2 ± 0.3

4.4.2 Screening of extractants

Of the extractants tested in the screening (Table 2, page 12), Cyanex 272, Cyanex 923 and TBP gave distribution ratios which were too low to quantify ($<10^{-3}$) with our method. The organic phases in the screening consisted of 0.2 M extractant in kerosene. Each organic phase was contacted with three aqueous phases, as described in section 3.4. After the tracer solution had been added, the aqueous phases used in the screening consisted of:

1. 0.53 M HNO_3 and 0.5 M H_3PO_4 (pH=0.3)
2. 0.12 M HNO_3 and 0.05 M H_3PO_4 (pH=0.9)
3. 0.08 M HNO_3 and 0.005 M H_3PO_4 (pH=1.1)

Figure 21 shows the results obtained with HDEHP. In addition to the experiments performed as part of the screening, extraction was done from a mixture of 0.08 M HNO_3 and 0.005 M H_3PO_4 was neutralized to pH=2 by addition of concentrated NH_4OH. This gave a distribution ratio of 0.7, which was considered high enough to warrant further study of HDEHP. The distribution ratio measured at pH=0.3 was too low to quantify ($<10^{-3}$). Very low distribution ratios give very low count rates from the organic phase. When the count rate approaches the count rate due to noise (the background), it becomes very difficult to quantify the fraction of the count rate that is due to ^{109}Cd. The same is true

for very high distribution ratios, which lead to low count rates from the aqueous phase. In this work, distribution ratios ranging from 10^{-3} to 10^{3} were measured confidently. This range could perhaps have been widened with a higher radioactivity concentration in the tracer solution.

4.4.3 HDEHP

Figure 22 is a plot of the percent extracted as a function of stirring time for 0.2 M HDEHP and Cyanex 301. It shows that with both extractants, equilibrium was established within two minutes. Figure 23 is an equivalent plot, where the variable is the time the two phases were contacted by shaking on a shaking table. In Figure 23, 1.0 M HDEHP had been used, and that is why the percent extracted is higher than in Figure 22. The figures show that by either stirring or shaking, equilibrium is reached within five minutes. In order to be sure that equilibrium was achieved, the phases were shaken for ten minutes in subsquent experiments.

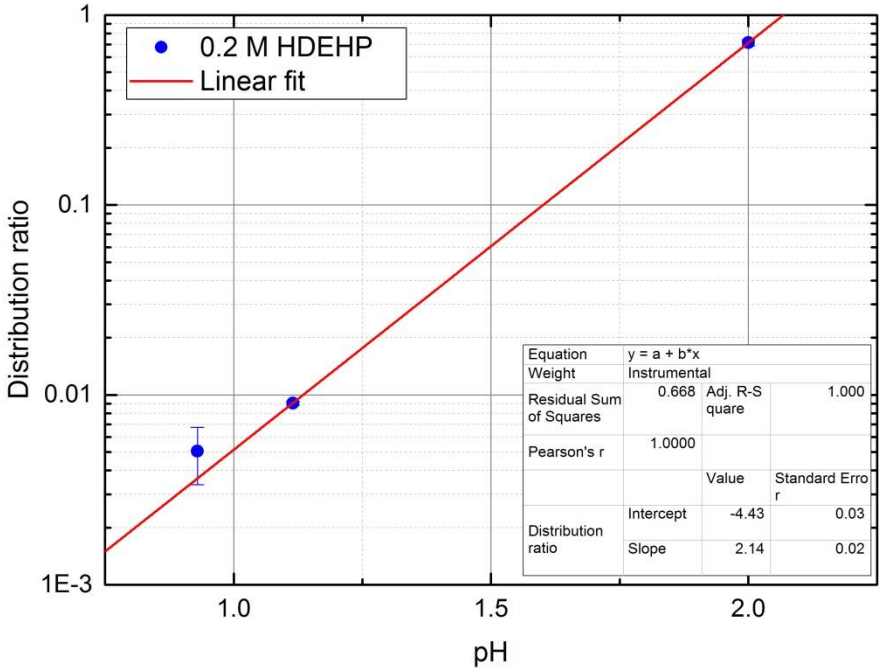

Figure 21: The distribution ratio of Cd observed with 0.2 M HDEHP in kerosene as organic phase. Aqueous phase: 0.12 M HNO_3 and 0.05 M H_3PO_4 (pH=0.9), 0.08 M HNO_3 and 0.005 M H_3PO_4 (pH=1.1) and 0.08 M HNO_3 and 0.005 M H_3PO_4 neutralized with NH_3 (pH=2.0).

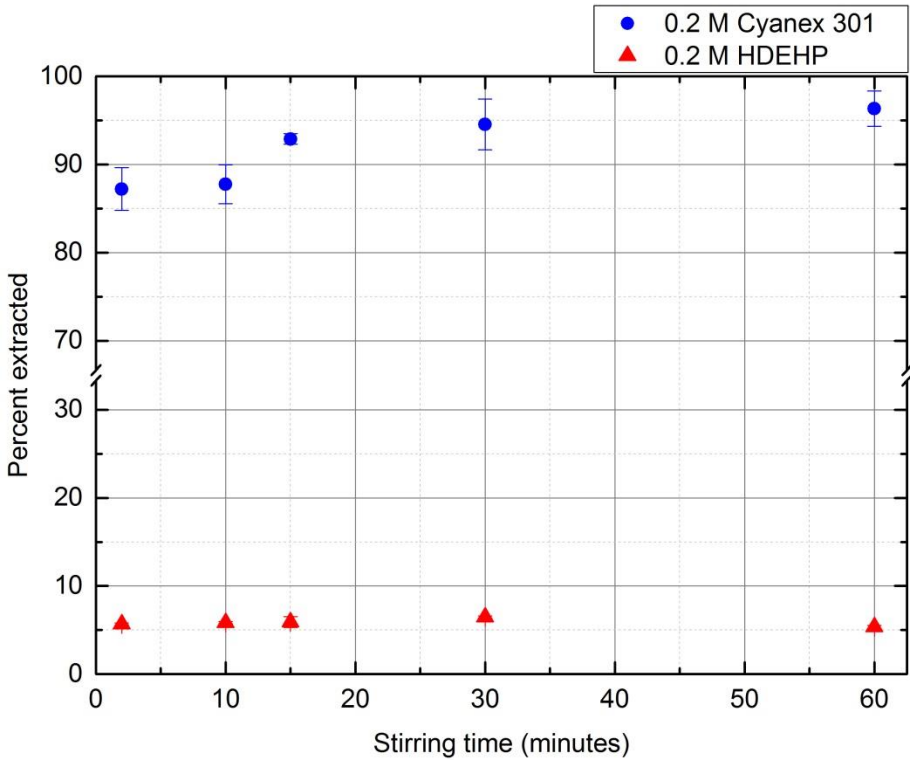

Figure 22: Percent Cd extracted as function of stirring time. Organic phase: 0.2 M HDEHP in kerosene. The aqueous phase consisted of 0.04 M HNO_3 and 0.005 M H_3PO_4, giving pH=1.5.

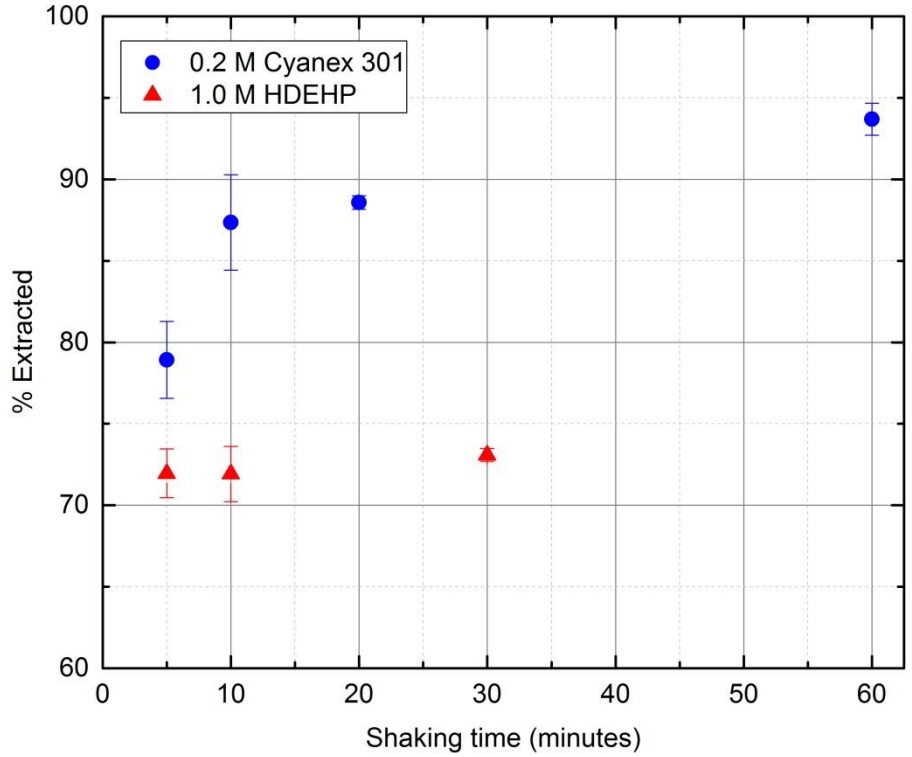

Figure 23: Percent Cd extracted as functions of shaking time for 1.0 M HDEHP in kerosene. The percent extracted is higher than in Figure 22 because the concentration of HDEHP is higher. The aqueous phase consisted of 0.04 M HNO_3 and 0.005 M H_3PO_4, giving pH=1.5.

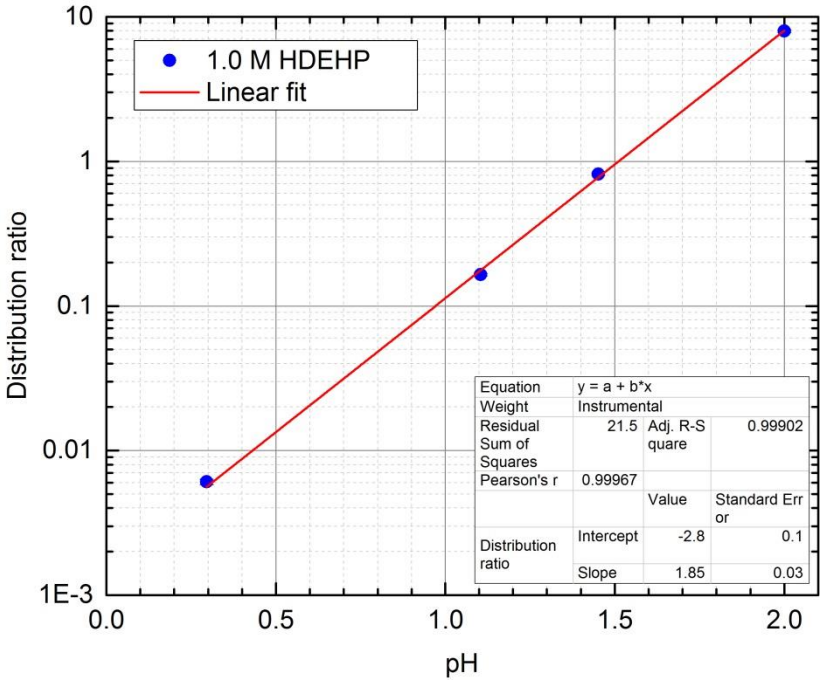

Figure 24: Distribution ratio of cadmium obtained with 1.0 M HDEHP. Aqueous phase: 0.5 M HNO_3 and 0.5 M H_3PO_4 (pH=0.3), 0.08 M HNO_3 and 0.05 M H_3PO_4 (pH=1.1), 0.04 M HNO_3 and 0.005 M H_3PO_4 (pH=1.5) and 0.04 M HNO_3 and 0.05 M H_3PO_4 neutralized with NH_3 (pH=2.0).

Figure 24 shows the distribution as function of pH when using 1.0 M HDEHP. With 0.2 M and 1.0 M HDEHP, the slopes of $\log D$ as functions of pH equal 2.14 ± 0.02 and 1.85 ± 0.03, respectively. This is as expected from the way a cation-exchanging extractant reacts with a divalent cation (Eq. 11, page 13). Figure 25 is a plot of the distribution ratio as a function of HDEHP concentration. The slope is 2.15 ± 0.04. Based on equations 11, 12 and 14, one can therefore conclude that the following reaction takes place between HDEHP (HA) and Cd^{2+}:

$$Cd^{2+}(aq) + 2HA(org) \rightleftharpoons CdA_2(org) + 2H^+(aq) \qquad \text{Eq. 30}$$

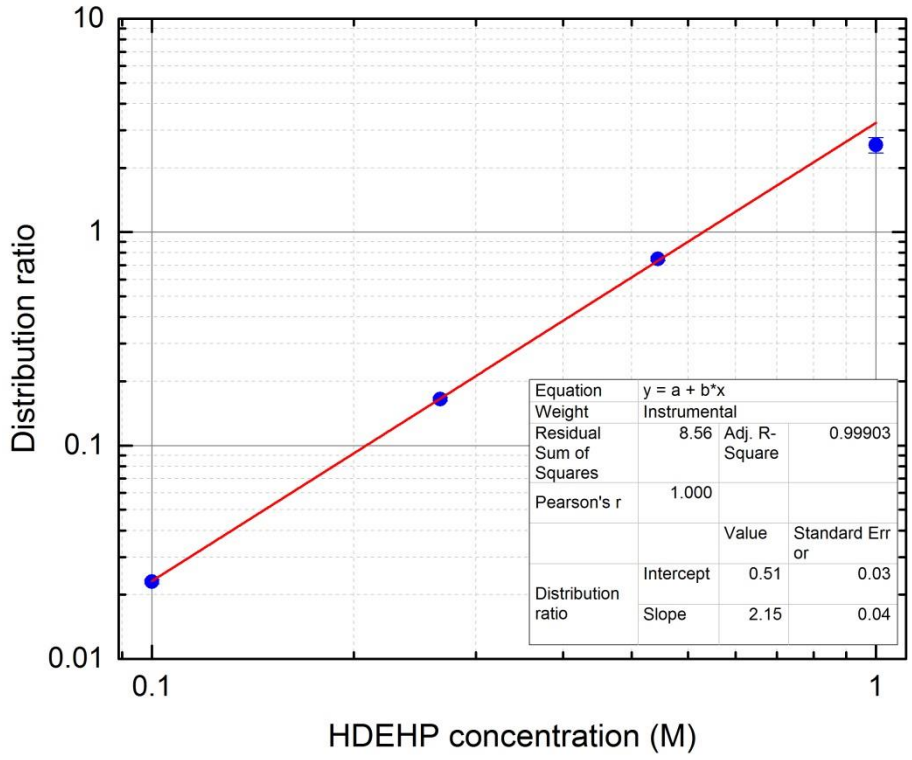

Figure 25: Distribution ratio of Cd as function of HDEHP concentration. Aqueous phase: 0.04 M HNO_3 and 0.005 M H_3PO_4.

Figure 26 shows the results of using a mixture containing 0.5 M HDEHP and 0.5 M TBP in kerosene as organic phase. The results are plotted along with the results from using 0.2 M and 1.0 M HDEHP. The figure shows that the distribution ratio does not increase significantly when TBP is present. On the contrary, 0.5 M HDEHP and 0.5 M TBP give approximately same results as one would expect from 0.5 M HDEHP alone, based on the previous results, i.e. somewhere between the distribution ratios obtained with 0.2 and 1.0 M HDEHP. Ideally, an experiment using 0.5 M HDEHP without TBP should have been performed, in order to look for small effects from having TBP present. Nevertheless, Figure 26 shows that TBP does not significantly increase the distribution ratio.

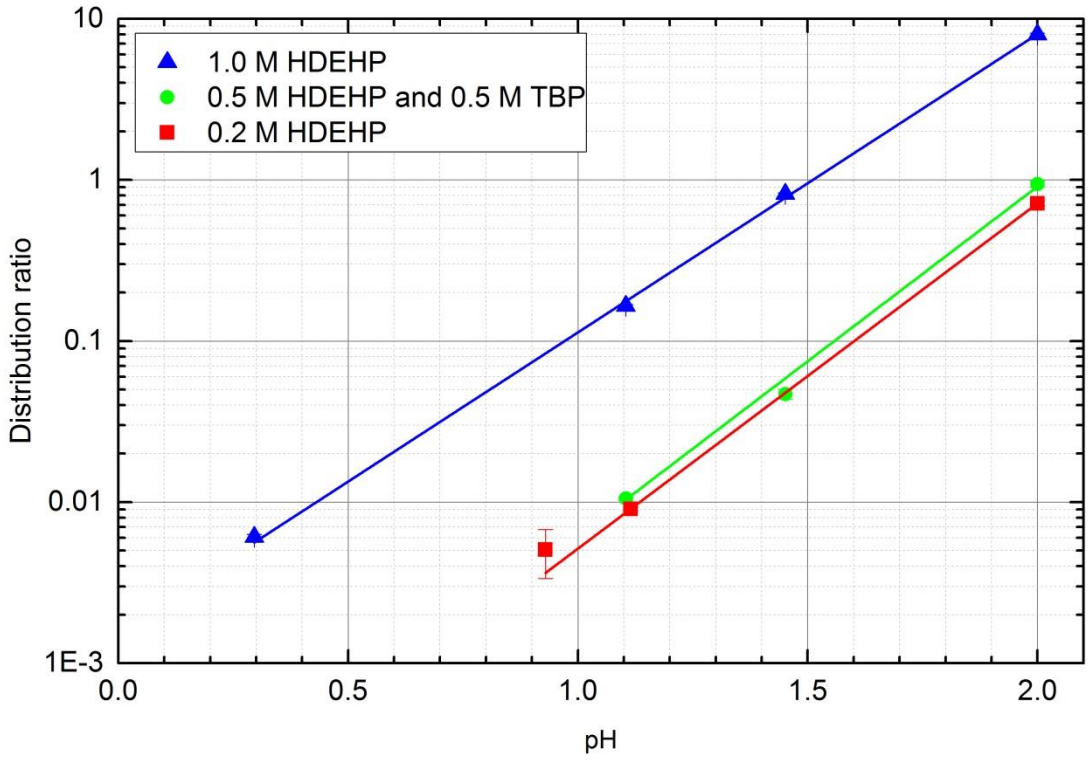

Figure 26: The results obtained with an organic phase consisting of 0.5 M HDEHP and 0.5 M TBP, plotted alongside with the results obtained with 1.0 M HDEHP and 0.2 M HDEHP, without TBP. The aqueous phases in the experiments with 0.5 M HDEHP and 0.5 M TBP were 0.08 M HNO_3 and 0.05 M H_3PO_4 (pH=1.1), 0.04 M HNO_3 and 0.005 M H_3PO_4 (pH=1.5) and 0.04 M HNO_3 and 0.005 M H_3PO_4 neutralized with NH_3 (pH=2.0).

Based on the distribution ratios plotted in Figure 24, one can envision a system for industry-scale extraction of cadmium (Figure 27). In such a system, one could increase the pH in the mother liquor to 1.5 by adding ammonia gas, i.e. just add a little more NH_3 than Yara currently does. At pH=1.5, one could extract cadmium and other metal cations by using 1.0 M HDEHP in kerosene. One would need to control the pH by adding ammonia during extraction. According to Figure 24, this should give a distribution ratio of 1. One could in turn strip the organic solution by contacting it with e.g. 1.0 M HNO_3. This should give a distribution ratio under 0.01 for cadmium. Other cations, especially trivalent and tetravalent cations would probably be more strongly bound to HDEHP, and may require more concentrated acid or other stripping agents in order to be removed from the organic phase. The stripped organic phase could then be re-used to extract from neutralized mother liquor. The metal cations could be removed from the HNO_3 used to strip the organic solution by passing the HNO_3 through an ion exchange column. Finally, one could separate the different metals by selectively eluting them from the column. In such a system, solvent extraction would in effect serve as a means to remove the metals from the matrix of the mother liquor, which contains undissolved matter that could clog an ion exchange column.

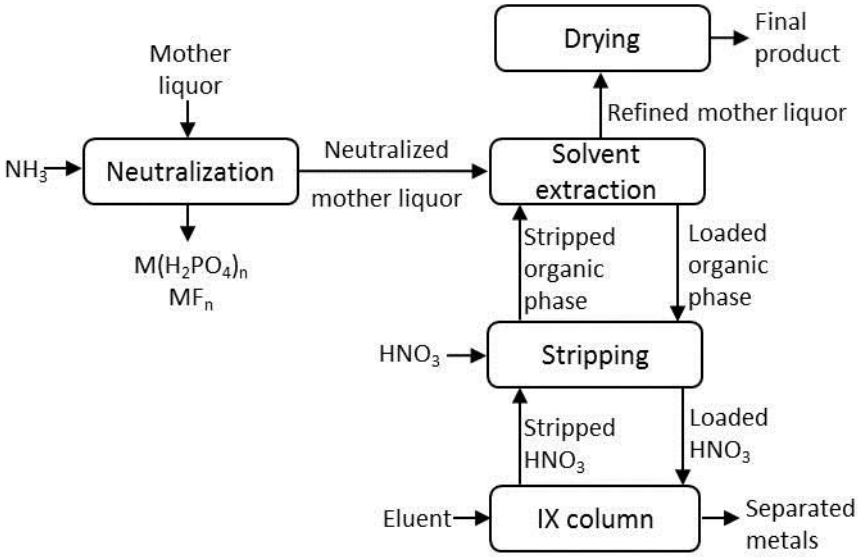

Figure 27: Sketch of how solvent extraction can be used to remove Cd and other metals from mother liquor. The diagram also includes a stage for the separation of the various metals from each other by using an ion exchange (IX) column.

However, extraction from mother liquor did not work as well as from dilute solutions of nitric and phosphoric acid. When attempting to extract cadmium from mother liquor using 1.0 M HDEHP, a distribution ratio of only 0.048 ± 0.001 was measured at an equilibrium pH of 2.3. This is significantly lower than the results obtained when extracting cadmium from a dilute mixture of nitric and phosphoric acid (Figure 24). This may be because HDEHP extracts many of the other metal cations present in the mother liquor. HDEHP is one of the most common and widely used extractants in hydrometallurgy, and is known to be able to extract a number of metal cations, including cobalt, nickel, chromium, vanadium and zinc [20], all of which are present in the mother liquor (Table 4, page 39). 1.0 M HDEHP has too low capacity to extract cadmium in one extraction stage and with a phase ratio of 1. In other words, HDEHP is not selective enough to efficiently extract cadmium.

One could perform several extraction stages, meaning that one could mix the aqueous phase with the organic phase, separate the phases and then mix the aqueous phase with a fresh volume of organic phase. In the first stage, the cations that have the highest affinity for HDEHP (typically those that have high charge density) would be extracted. The remaining metals could then more efficiently be removed in the second stage. However, the iron concentration of 2.17 M alone (Table 4) is so high that it would require several extraction stages with a phase ratio of 1 to remove it.

Moreover, when mother liquor was neutralized to pH=1.5, so much precipitate formed that less than half of the initial volume of the solution remained. Dealing with that much precipitate on an industrial scale would be expensive. One would need to re-dissolve it in acid in order to recover the

phosphate and somehow separate the phosphate from the toxic metals. Overall, the results show that 1.0 M HDEHP by itself is probably not suited to extract cadmium from mother liquor in a single step.

However, there may be some way of increasing the selectivity and distribution ratio of the cadmium-HDEHP complex. For example, Takeshita et al. found that N,N,N,N-tetrakis (2-pyridylmethyl)ethylene diamine (TPEN) could work as a synergist for extracting cadmium with HDEHP [35]. They found that the distribution ratio of cadmium increased by approximately an order of magnitude when TPEN was present in the aqueous phase. The distribution ratio of zinc, on the other hand, decreased, meaning that the separation factor, i.e. the distribution ratio of cadmium divided by the distribution ratio of zinc increased 500-fold. However, TPEN is a hexadentant ligand with nitrogen donors, and is protonated at low pH. This could make it unsuitable for extraction from mother liquor. Either way, this is an example of how different compounds such as HDEHP and TPEN can be used in tandem in order to produce synergistic effects. Alternatively, one could attempt to discover or produce a selective extractant for cadmium. However, this is difficult and time consuming. Such an extractant would have to not only extract cadmium, but also withstand the oxidative conditions present in the mother liquor. The following section illustrates the importance of this issue.

4.4.4 Cyanex 301

Figure 28 is a plot of the distribution ratios obtained with 0.2 M Cyanex 301 when extracting cadmium from a mixture of synthetic nitric and phosphoric acid. The plot shows that Cyanex 301 is a very effective extractant of cadmium, with high distribution ratios in the entire pH range. The distribution ratio decreases with increasing pH. This is contradictory to the assumption that Cyanex 301 is a cation-exchanging extractant, and was therefore a surprise. In order to see if the effect was a result of changing nitrate concentration, the experiment was carried out with a constant nitric acid concentration (0.5 M). pH was adjusted by adding concentrated NH_4OH-solution. This led to similar results (Figure 29). Again, the distribution ratio decreased with pH.

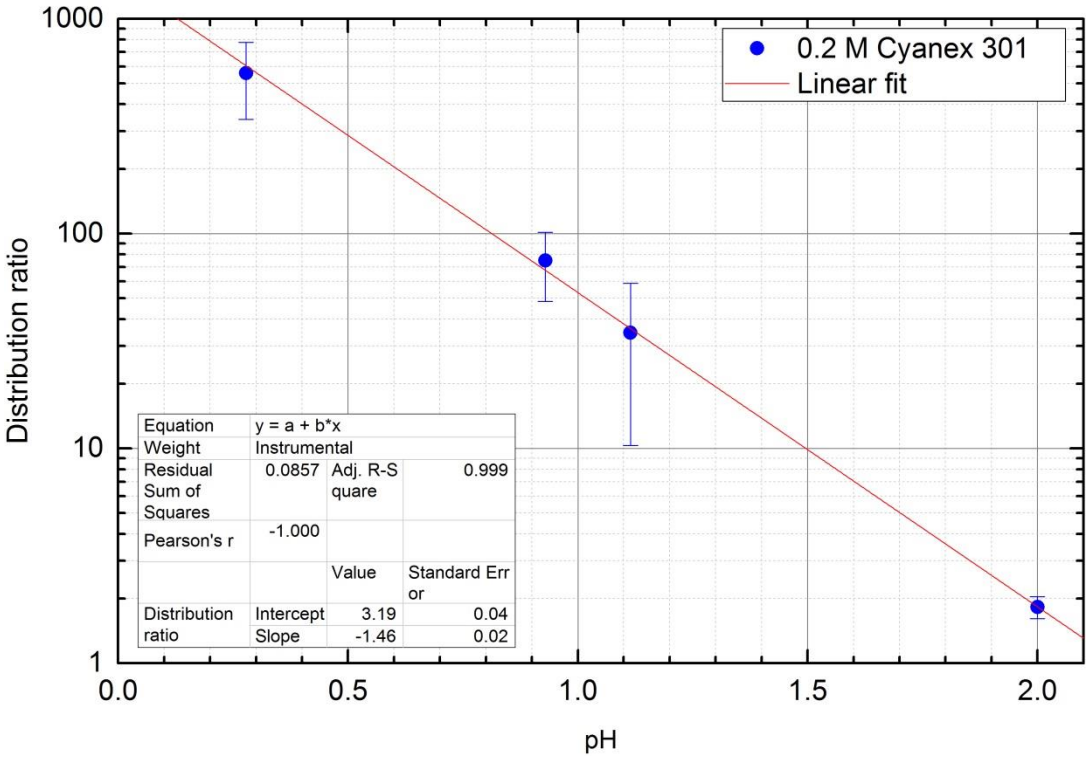

Figure 28: Distribution ratios obtained with 0.2 M Cyanex 301. Aqueous phase: 0.5 M HNO_3 and 0.5 M H_3PO_4 (pH=0.3), 0.08 M HNO_3 and 0.05 M H_3PO_4 (pH=0.9), 0.04 M HNO_3 and 0.005 M H_3PO_4 (pH=1.1) and 0.04 M HNO_3 and 0.005 M H_3PO_4 neutralized with NH_3 (pH=2.0).

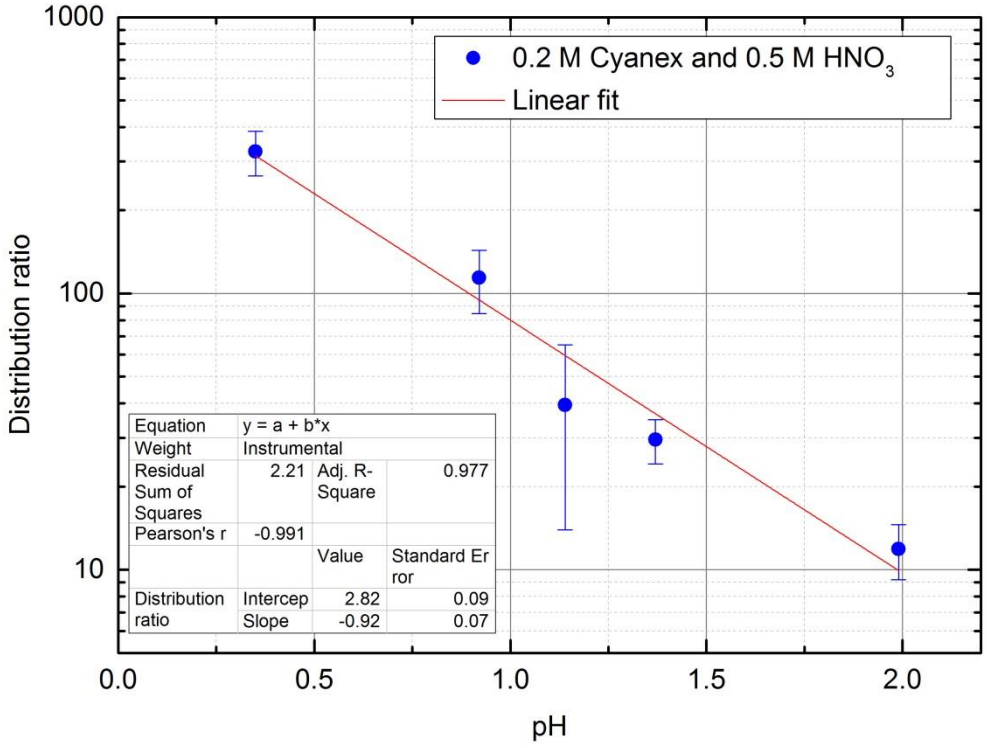

Figure 29: The results obtained when extracting cadmium from 0.5 M HNO_3, using 0.2 M Cyanex 301 in kerosene as the organic phase.

A plausible explanation to these results could be that Cyanex 301 does not work as a cation exchanger in nitric acid media. Instead, one can speculate that it works in the following way:

Dag Eriksen suggested that Cyanex 301 (R_2PSSH) might react as a base with nitric acid [36]:

$$R_2PSSH\ (org) + HNO_3\ (aq) \rightleftharpoons R_2P(SH)_2NO_3\ (org) \qquad \text{Eq. 31}$$

The equilibrium constant for this reaction would be:

$$K_1 = \frac{[R_2P(SH)_2NO_3]_{org}}{[R_2PSSH]_{org}[HNO_3]_{aq}} \qquad \text{Eq. 32}$$

Then, one can suppose that cadmium forms a negative nitrate complex, and that this negative complex can react with two $R_2P(SH)_2NO_3$-compexes, similar to how a negative complex can be extracted by a tertiary amine (anion exchange):

$$Cd^{2+}\ (aq) + 4\ NO_3^-\ (aq) \rightleftharpoons [Cd(NO_3)_4]^{2-}\ (aq) \qquad \text{Eq. 33}$$

$$[Cd(NO_3)_4]^{2-}\ (aq) + 2R_2P(SH)_2NO_3\ (org) \rightleftharpoons Cd(NO_3)_4(R_2P(SH)_2)_2\ (org) + 2NO_3^-\ (aq) \qquad \text{Eq. 34}$$

Adding equations 31, 33 and 34 together gives the net reaction of this process:

$$Cd^{2+}\ (aq) + 2R_2PSSH\ (org) + 2H^+\ (aq) + 4\ NO_3^-\ (aq) \rightleftharpoons Cd(NO_3)_4(R_2P(SH)_2)_2\ (org) \qquad \text{Eq. 35}$$

The equilibrium constant for this reaction would be:

$$K_{net} = \frac{[Cd(NO_3)_4(R_2P(SH)_2)_2]_{org}}{[Cd^{2+}]_{aq}[R_2PSSH]_{org}^{\ 2}[H^+]_{aq}^{\ 2}[NO_3^-]_{aq}^{\ 4}} \qquad \text{Eq. 36}$$

Inserting $D = \frac{[Cd(NO_3)_4(R_2P(SH)_2)_2]_{org}}{[Cd^{2+}]_{aq}}$, taking the logarithm and for simplicity removing the subscripts for the phases gives:

$$\log K_{overall} = \log D - 2\log[R_2PSSH] - 2\log[H]^+ - 4\log[NO_3^-] \qquad \text{Eq. 37}$$

Solving for D and introducing $\mathrm{pH} = -\log[\mathrm{H}^+]$ gives:

$$\log \mathrm{D} = \log \mathrm{K}_{\mathrm{overall}} - 2\mathrm{pH} + 2\log[\mathrm{R}_2\mathrm{PSSH}] + 4\log[\mathrm{NO}_3^-] \qquad \text{Eq. 38}$$

Therefore, with constant concentrations of Cyanex 301 and nitrate, one would expect $\log \mathrm{D}$ to decrease as a function of pH, with a slope of -2. The fact that the observed slope is less steep could be because that at lower pH, oxidation of Cyanex 301 becomes more significant, which works to decrease the concentration of Cyanex 301 and thereby reduce the distribution ratio.

The results in Figure 30 were also surprising. This plot shows that the distribution ratio decreases with increasing concentration of Cyanex 301, when one would expect it to increase regardless of whether it worked as a cation exchanger or through the process described above. If Cyanex 301 could take part in only one reaction, which was to extract cadmium, the le Châtellier principle would require the distribution ratio to increase when more Cyanex 301 was added. However, as explained in section 2.4 , Cyanex 301 is oxidized to a dimer in the presence of nitrate:

$$2R_2PSSH\ (org) + 2HNO_3\ (aq) \rightleftharpoons R_2SP\text{-}S\text{-}S\text{-}PSR_2\ (org) + 2NO_2\ (aq) + 2H_2O\ (l) \qquad \text{Eq. 39}$$

The produced dimer (R_2SP-S-S-PSR_2) does not extract cadmium. This means that when a molecule of Cyanex 301 is added to the organic phase, it can either work to extract cadmium or it can react with another molecule of Cyanex 301 and form a dimer. If a dimer is formed, the net result of adding one molecule of Cyanex 301, is to in fact reduce the concentration of Cyanex 301 and shift the equilibrium in Eq. 35 (page 51) to the left. This would also be true if Cyanex 301 extracted cadmium as a cation exchanger. The equilibrium constants of the extraction and oxidation reactions, respectively, would decide which of the two reactions that controlled the system, as long as equilibrium was established. Figure 22 shows that equilibrium was established. The fact that the distribution ratio in Figure 30 decreases with increasing Cyanex 301 concentration indicates that the equilibrium constant of the oxidation is greater than that of the extraction.

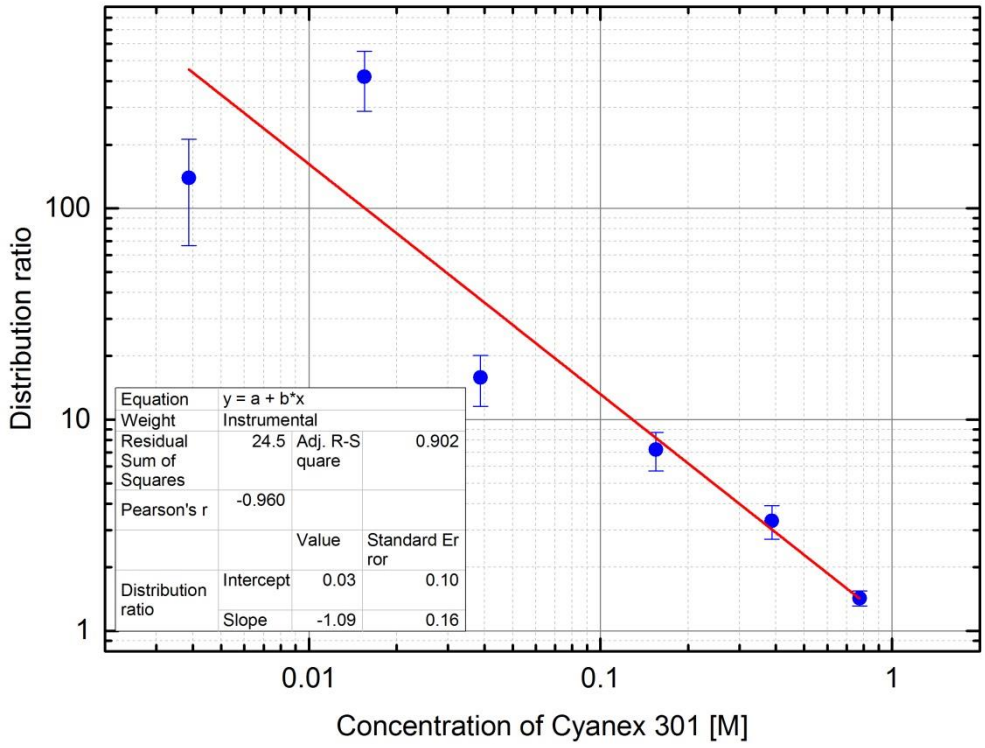

Figure 30: Distribution ratios obtained with different concentrations of Cyanex 301. The aqueous phase in each experiment consisted of 0.02 M HNO_3 and 0.005 M H_3PO_4 (pH=1.7).

In order to check whether increasing the Cyanex 301 concentration leads to more dimerization rather than more extraction, one could repeat the experiments done in this work, and use $^{31}P\{^1H\}$ NMR to measure the dimerization, the way Marc et al. analyzed the dimerization of Cyanex 301 in reference [31]. Judging by that article, $^{31}P\{^1H\}$ NMR could probably also be used to measure whether Cyanex 301 is really protonated by nitric acid, the way Eq. 31 (page 51) proposes that it is.

5 Conclusion

A method for the production of a radioactive tracer for cadmium was successfully developed and implemented. One of the benefits of using this method is that irradiation of the silver target can be combined with other experiments at the cyclotron lab that use ^{4}He projectiles, without added cost. The cadmium produced as a result of irradiation was selectively and safely removed from the silver target. The method could be improved by finding a more effective way to condense the cadmium in the helium gas flow, and to wash it into a smaller volume of acid than what was used in this work. That would increase the radioactivity concentration in the final radiotracer solution. Nevertheless, the method at large works and the produced radiotracer solution was suitable for solvent extraction experiments. Project goal 1 was achieved.

The way cadmium distributes between the precipitate and the remaining solution in the neutralization step of the Odda process was successfully investigated by using ^{109}Cd as a radioactive tracer. Gamma spectroscopy was used to measure the respective relative concentrations of ^{109}Cd in the precipitate and the solution. The results show that in the pH-range of 1.0-1.5, the mass concentrations of cadmium in the precipitate and the solution are equal. The cadmium is incorporated into the bulk volume of the precipitate, probably as part of a crystal structure. Project goal 2 was achieved.

A literature review was undertaken in order to look for potential industrial extractants that could be suitable for solvent extraction of cadmium from mother liquor. Some selected extractants were tested with dilute solutions of nitric and phosphoric acid. Of these, HDEHP and Cyanex 301 were effective enough to warrant further investigation. The reactions between the extractants and Cd^{2+} were investigated by using the radioactive tracer produced at the cyclotron. The distribution ratio of cadmium was determined by measuring the concentration of ^{109}Cd in the organic and aqueous phases, respectively. LSC was used to measure the radiation from ^{109}Cd. To do so, a method was developed to correct for differences in quenching.

The methods used in the solvent extraction experiments were effective. The shaking table made it possible to run several experiments at the same time. The work could have been done more efficiently if one could have shaken and centrifuged the phases in the same vial. Nevertheless, the method should be useful for performing other solvent extraction experiments. LSC gives a high counting efficiency and therefore a relatively short counting time for the detection of ^{109}Cd. That made it possible to measure the results of several experiments overnight. ^{109}Cd could be used as a radioactive tracer in other work investigating the behavior of cadmium in liquids. Alternatively, ^{109}Cd

could be made part of a larger molecule which then could be used as a radioactive tracer. In either case, one should consider LSC as a possible means of detection.

The results from the solvent extraction experiments show that 1.0 M HDEHP extracts cadmium effectively from pure synthetic solutions of nitric and phosphoric acid. Adding TBP did not cause a synergistic effect.

The results obtained with HDEHP and synthetic solutions of nitric and phosphoric acid suggest that HDEHP could be used to extract cadmium on an industrial scale. However, extraction is less effective from an actual fertilizer-production solution. This could be due to the presence of many other metal cations in the solution and their competition for bonding to HDEHP. Nevertheless, the results could form the foundation for further work investigating HDEHP as an extractant of cadmium, perhaps in synergy with another ligand. Such a ligand could work as a masking agent for some of the other cations present in the mother liquor, particularly for iron, so that HDEHP became more selective. Ideally, one should find a way to extract cadmium bellow pH 1, in order to avoid precipitation of metal dihydrogen phosphates. That may require using another extractant than HDEHP.

Future work on solvent extraction of cadmium from mother liquor could also focus on trying to eliminate iron and other non-toxic cations before solvent extraction. That would make a lot more of the extractant available for extraction of cadmium. It would also be interesting to study solvent extraction of cadmium from dilute solutions of nitric and phosphoric acid containing increasing concentrations of other cations than cadmium, such as those listed in Table 4 (page 39). That would give more information about why extraction is less effective from mother liquor than from dilute solutions.

The ability of Cyanex 301 to extract cadmium from a mixture of nitric and phosphoric acid was studied, and a hypothesis that could explain the observations was outlined. While other authors have reported that Cyanex 301 works as a cation exchanger when it extracts cadmium from phosphoric acid, the results in this work suggest that Cyanex 301 behaves more like an anion exchanger in the presence of nitric acid. In the presented hypothesis, oxidation of Cyanex 301 by nitric acid leads to the effect that increasing the concentration of Cyanex 301 decreases the distribution ratio. The results obtained with Cyanex 301 were unexpected, and further work is required in order to confirm the presented hypothesis. $^{31}P\{^{1}H\}$ NMR could probably be useful in that work.

Both HDEHP and Cyanex 301 can extract cadmium effectively under the right circumstances. However, HDEHP is not selective enough and Cyanex 301 is oxidized by the mother liquor. Overall, project goal 3 was only partially achieved.

Appendix 1: List of chemicals and producers

Chemical	**Producer**
HNO_3	KEBO Lab
HCl	Merck
NH_3 gas	Linde
NH_4OH solution	VWR
Asol D80 (Kerosene)	Univar AS
HDEHP	Lanxess
NaOH, 0.25 M Titrisol	Merck
HDEHP	Lanxess
Cyanex 301/272/923	Cytec
TBP	Lanxess
Gold Star LSC-cocktail	Meridian Biotechnologies
Instagel Plus	Perkin Elmer

Appendix 2: Calculation of cyclotron-produced radioactivities of ^{109}Cd and ^{109}In

Figure 7 shows the result of a calculation of the ^{109}Cd and ^{109}In produced in a 1 mm thick silver disk during irradiation with a beam of ^{4}He-particles. The simulated beam current (equivalent to beam flux) was set to 400 nano-Amperes (nA), which is a common beam current for ^{4}He-particle beams. The cross section for the ^{107}Ag(α,2n)^{109}In-reaction was set to 1 barn, based on Figure 5. The plotted radioactivities were calculated in the following way:

During irradiation the rate at which ^{109}In-atoms are generated equals:

$$R_{form.,In} = \sigma\phi N_T \qquad \text{Eq. 40}$$

σ is the cross-section of the the ^{107}Ag(α,2n) ^{109}In -reaction, ϕ is the flux of ^{4}He-particles and N_T is the number of ^{107}Ag-nuclides which lay in the path of the beam. At the same time as some ^{109}In is being generated, some of it disintegrates. The decay rate of ^{109}In equals:

$$A_{In} = \lambda_{In} N_{In} \qquad \text{Eq. 41}$$

$\lambda_{In} = \frac{\ln 2}{T_{1/2,In}}$ is given by the half-life of ^{109}In and is called the decay constant.

The rate of change in ^{109}In-nuclides equals the formation rate minus the decay rate:

$$\frac{dN_{In}}{dt} = \sigma\phi N_T - \lambda_{In} N_{In} \qquad \text{Eq. 42}$$

Integration of Eq. 42 gives N_{In}. The rate of formation of ^{109}Cd equals the decay rate of ^{109}In:

$$R_{form.,Cd} = A_{In} \qquad \text{Eq. 43}$$

The expression for the rate of decay of ^{109}Cd is similar to that for ^{109}In:

$$A_{Cd} = \lambda_{Cd} N_{Cd} \qquad \text{Eq. 44}$$

Combining equations 43 and 44 gives the rate of change of number of cadmium nuclides:

$$\frac{dN_{Cd}}{dt} = \lambda_{In} N_{In} - \lambda_{Cd} N_{Cd} \qquad \text{Eq. 45}$$

Equations 42 and 45 were integrated numerically in order to find N_{In} and N_{Cd}, respectively. Equations 41 and 44 were used to calculate the decay rates of ^{109}In and ^{109}Cd, respectively, when the cyclotron beam was on. When the beam was of, we the radioactivities decreased according to their decay rates:

$$A_{Cd} = A_0 \cdot e^{-\lambda t_{off}} \qquad \text{Eq. 46}$$

t_{off} represents the time since the beam was turned off and A_0 is the radioactivity when the beam was turned off.

The two following MATLAB-scripts were written to simulate the radioactivity content in the disk during irradiation. The script Ingrowth.m calculates the radioactivities when the beam is on. CD_In_decay.m calculates the radioactivities when the beam is off.

Ingrowth.m:

```
function [ t, D_Cd,D_In ] = Ingrowth(hours, D_Cd0, D_In0,t0,nt)
%INGROWTH: This function calculates the radioactivities of 109Cd and 109In
%as functions of time as they grow in a disk of natural silver which is being
%irradiated with 4He-particles. The beam current is set to 400 nA and the
%cross section for the 107Ag(a,2n)109In-reaction is set to 1 barn.
%Inputs:
%   hours: The time during which the decay proceeds
%   D_Cd0: The initial radioactivity of 109Cd
%   D_In0: The initial radioactivity of 109In
%   t_0:   The initial time
%   n_t:   The number of time intervals into which to separate "hours"

T109In=4.2;                     %Half-life in units of hours
T109In=T109In*3600;             %Half-life in units of seconds
sigma=1;                        %Cross section in units of barn
sigma=sigma*10^-24;             %Cross section in units of cm^2
d=0.1;                          %Thickness of silver disk in units of cm
ad=5.86e21;                     %Areal density of Ag in units of cm^-2
beamcurrent=400e-9;             %Beam current in units of Amperes
lambda_Cd=log(2)/462/24/3600;   %Decay constant in units of s^-1 for 109Cd
lambda_In=log(2)/T109In;        %Decay constant in units of s^-1 for 109In

%Produce an array of time in units of seconds:
seconds=hours*3600;
dt=seconds/(nt-1);
t=t0:dt:t0+seconds;
```

```
a_flux=beamcurrent/2*6.24e18;    %Flux of 4-He given by the beam current
                                 %multiplied with the number of elemental
                                 %charges per Coulomb divided by two.

form_rate_In=sigma*a_flux*ad*0.5183; %Rate of formation of 109In

%Produce arrays for the number of nuclides of 109Cd and 109In of equal
%length as that for time
n=length(t);
N_Cd=zeros(n,1);
N_In=zeros(n,1);

%Fill the initial elements of the arrays based on the inputs
N_In(1)=D_In0/lambda_In;
N_Cd0=D_Cd0/lambda_Cd;
N_Cd(1)=N_Cd0;

%Fill the arrays
for i=1:n-1
    %The change in the number of 109Cd-nuclides in a time dt equals those
    %generated by the decay of 109In minus those that decay:
    dN_Cd=(N_In(i)*lambda_In-lambda_Cd*N_Cd(i))*dt;
  N_Cd(i+1)=N_Cd(i)+dN_Cd;
  %The change in the number of 109In-nuclides in a time dt equals those
    %generated by the irradiation minus those that decay:
    dN_In=(form_rate_In-lambda_In*N_In(i))*dt;
    N_In(i+1)=N_In(i)+dN_In;
end
%Produce arrays of the radioactivities of 109Cd and 109In, respectively
D_Cd=N_Cd*lambda_Cd;
D_In=N_In*lambda_In;

%Convert the time array to a column vector:
t=transpose(t);
end
```

Cd_In_decay.m:

```
function [ t, D_In, D_Cd ] = Cd_In_decay( hours, D_In0, D_Cd0, t_0,nt )
%CD_IN_DECAY: This function calculates the radioactivities of 109Cd and
%109In as functions of the time while the two isotopes decay.
%Inputs:
%   hours: The time during which the decay proceeds
%   D_In0: The initial radioactivity of 109In
%   D_Cd0: The initial radioactivity of 109Cd
%   t_0:   The initial time
%   n_t:   The number of time intervals into which to separate "hours"

seconds=hours*3600;     %find the number of seconds equivalent to the input hours
dt=seconds/(nt-1);      %find the increment time
t=0:dt:seconds;         %build an array of time
lambda_Cd=log(2)/(462*24*3600);  %decay constant in of s^-1

n=length(t);
```

```
D_In=zeros(n,1);        %Empty array of decay rate of Indium
D_Cd=zeros(n,1);        %Empty array of decay rate of Cadmium
N_Cd=zeros(n,1);        %Empty array of number of Cd atoms

N_Cd(1)=D_Cd0/lambda_Cd;
D_Cd(1)=D_Cd0;
D_In(1)=D_In0;

%Fill the arrays
for i=2:n
    %The radioactivity of 109In decays according to its half-life
    D_In(i)=D_In0*0.5^(t(i)/(3600*4.2));
    %The increase in the number of 109Cd-nuclides in the time dt equals the
    %decay rate of 109In minus the decay rate of 109Cd:
    N_Cd(i)=N_Cd(i-1)+(D_In(i)-lambda_Cd*N_Cd(i-1))*dt;
  D_Cd(i)=N_Cd(i)*lambda_Cd;
end

%Convert the time array to a column vector:
t=transpose(t+t_0*3600);
end
```

Appendix 3: Calculation of uncertainties

The uncertainty σ in a measurement of radioactivity equals the square root of the number of counts N_C:

$$\sigma_N = \sqrt{N_C} \qquad \text{Eq. 47}$$

The count rate R equals the number of counts divided by the counting time t:

$$R = \frac{N_C}{t} \qquad \text{Eq. 48}$$

Similarly, the uncertainty in the count rate equals:

$$\sigma_R = \frac{\sigma_N}{t} \qquad \text{Eq. 49}$$

The amount of radioactivity (the decay rate) A in a sample depends on both the observed count rate and the detector efficiency, ϵ:

$$A = \frac{R}{\epsilon} \qquad \text{Eq. 50}$$

The general formula for the relative standard error of a fraction $f = \frac{x}{y}$ is $\frac{\sigma_f}{f} = \sqrt{\left(\frac{\sigma_x}{x}\right)^2 + \left(\frac{\sigma_y}{y}\right)^2}$. This formula gives the following expression for the uncertainty in the radioactivity:

$$\sigma_A = A\sqrt{\left(\frac{\sigma_R}{R}\right)^2 + \left(\frac{\sigma_\epsilon}{\epsilon}\right)^2} \qquad \text{Eq. 51}$$

$\frac{\sigma_\epsilon}{\epsilon}$ is the relative standard error of the detector efficiency. Similarly, the uncertainty in the distribution ratio (Eq. 15, page 14) equals:

$$\sigma_D = D\sqrt{\left(\frac{\sigma_{A,org}}{A_{org}}\right)^2 + \left(\frac{\sigma_{A,aq}}{A_{aq}}\right)^2} \qquad \text{Eq. 52}$$

A_{org} is the radioactivity concentration in the organic phase, $\sigma_{A,org}$ is the uncertainty in A_{org}, and equivalently for A_{aq} and $\sigma_{A,aq}$ in the aqueous phase.

Appendix 4: Analysis of quench-series spectra

The following MATLAB-scripts were written in order to analyze the spectra from the various samples of different quenching. Calibrate_peak.m is the main script. The first few lines in each script contain a description of what that script does.

Calibrate_peak.m:

```
%Calibrate_peak.m: This scripts collects the spectra from three
%parallels stored in .xlsx-files contained in the same folder as the
%spectrum.

%Define the limits to the interval in which the Region of interest may
%start:
ROIstart1=0;
ROIstart2=0;
ROIend=1023;

%Read the spectra into three separate matrices:
[d1,~]=collect_spectra(pwd,0,1023,1);
[d2,~]=collect_spectra(pwd,0,1023,2);
[d3,~]=collect_spectra(pwd,0,1023,3);
%Find the maxima in the spectra:
[peak_max_channel1, ~ ]=FindPeakmax( d1 );
[peak_max_channel2, ~ ]=FindPeakmax( d2 );
[peak_max_channel3, ~ ]=FindPeakmax( d3 );

peak_max_channels=[peak_max_channel1; peak_max_channel2; peak_max_channel3];
a0=0; b0=0; rsq0=0;
l=length(peak_max_channel1);
E10=zeros(l); E20=zeros(l); E30=zeros(l);
sumcounts10=zeros(l); sumcounts20=zeros(l); sumcounts30=zeros(l);
E=zeros(length(peak_max_channels));

ROIstart0=0;
for ROIstart=ROIstart1:ROIstart2
    %Sum up the counts in the region of interest:
    sumcounts1=sumROI_single( d1,ROIstart,ROIend);
    sumcounts2=sumROI_single( d2,ROIstart,ROIend);
    sumcounts3=sumROI_single( d3,ROIstart,ROIend);
    %Calculate the mean number of counts in the unquenched samples:
    unq=1/3*(sumcounts1(1)+sumcounts2(1)+sumcounts3(1));
    %Calculate the relative efficicencies:
    E1=sumcounts1/unq;
    E2=sumcounts2/unq;
    E3=sumcounts3/unq;
    %Concatenate the efficiencies:
    E=[E1; E2; E3];
    %Fit the efficiencies to the peak maxima:
    m=fity_1(peak_max_channels,E);
    a=m(1); b=m(2); rsq=m(3);
    if rsq>rsq0
```

```
        a0=a; b0=b; rsq0=rsq;
        E10=E1;
        E20=E2;
        E30=E3;
        ROIstart0=ROIstart;
        sumcounts10=sumcounts1;
        sumcounts20=sumcounts2;
        sumcounts30=sumcounts3;
    end
end

%Calculate the fitted function
yfit=a0*peak_max_channels+b0;

%Plot the relative efficiency as a function of channel of peak max
figure
scatter(peak_max_channel1,E10, 'blue');
hold on
scatter(peak_max_channel2,E20, 'red');
scatter(peak_max_channel3,E30, 'green');
plot(peak_max_channels,yfit);
title(strcat('ROI starts at ', num2str(ROIstart0), '. R-squared: ',
num2str(rsq0)));
hold off
```

collect_spectra.m:

```
function [ double,triple] = collect_spectra(source_dir,
ROI_start,ROI_end,spec_num,filetype )
%TDCR_ROI This function collects the double- and triple coincidence spectra
%found in *.filetype-files in the source_dir-directory. spec_num
%indicates which spectrum to collect from a file, if several are present in
%each file.

%Collect the source files in a vector
sourcefiles= dir(fullfile(source_dir, filetype));

%Find the number of sourcefiles:
n=length(sourcefiles);

%Determine the number of channels to read
m=ROI_end-ROI_start+1;

%Create matrices in which to collect the double- and triple coincidence
%spectra as columns.

double=zeros(m,n);
triple=zeros(m,n);

%Find the first row iin the Excel file that contains the spectrum of
%interest.
firstrow=(spec_num-1)*1079+28;
```

```
%Find the first row in the Region of interest:
ch1=num2str(ROI_start+firstrow);
%Find the last row in the Region of interest:
ch2=num2str(ROI_end+firstrow);

%Create strings to designate which cells to read in from the file:
double_ch1=strcat('C',ch1);
double_ch2=strcat('C',ch2);
triple_ch1=strcat('E',ch1);
triple_ch2=strcat('E',ch2);
double_range=strcat(double_ch1,':',double_ch2);
triple_range=strcat(triple_ch1,':',triple_ch2);

%Read the cells of interest:
for i=1:n;
    filename=sourcefiles(i).name;
    double_column=xlsread(filename,double_range);
    triple_column=xlsread(filename,triple_range);
    for j=1:m
        double(j,i)=double_column(j);
        triple(j,i)= triple_column(j);
    end
end
```

FindPeakmax.m:

```
function [ peak_max_channel, peak_max_counts ] = FindPeakmax( spectra )
%FINDPEAKMAX This function finds the channel of the maximum of the highest
%peak in the spectra contained as columns in the input matrix "spectra".

[channels,numspectra]=size(spectra);

%Declare empty result arrays:
peak_max_channel=zeros(numspectra,1);
peak_max_counts=zeros(numspectra,1);

%Find the maximum in each spectrum:
for i=1:numspectra
    %Declare zero-values:
    count_max=0;
    channel_max=0;
    %Read the apropriate spectrum from the matrix:
    spectrum=spectra(:,i);
    %Find the maximum in the spectrum:
    for j=1:channels;
        %For each channel, read the number of counts:
        count=spectrum(j);
        %If the count number in the current channel is the highest so far,
        %then store it and the channel number:
        if count>count_max
            count_max=count;
            channel_max=j;
```

```
        end
    end
    %Store the maximum channel and counts of the spectrum in the apropriate
    %position in the result arrays:
    peak_max_channel(i)=channel_max;
    peak_max_counts(i)=count_max;
end
```

sumROI_single.m:

```
function [ sumcounts] = sumROI_single( spectra_matrix,ROI_start,ROI_end)
%SUMROI_single: This function sumarizes the counts in all the channels in
%a region of interest delimitated by the inputs ROI_start and ROI_end.
%Inputs:
%   spectra_matrix: The matrix containing the spectra, each column of which
%                   should represent an individual spectrum
%   ROI_start:      The first channel in the region of interest.
%   ROI_end:        The last channel in the region of interest.

%Find the size of the matrix:
d=size(spectra_matrix);
%Find how many spectra there are in the matrix:
d=d(2);
%Create an empty array of the sums:
sumcounts=zeros(d,1);

%For each spectrum j add the number of counts in the ROI:
for i=ROI_start+1:ROI_end+1
    for j=1:d
    sumcounts(j)=sumcounts(j)+spectra_matrix(i,j);
    end
end
```

fity_1.m:

```
function [ m ] = fity_1(x,y)
%FITY This function fits the vector y to a first-order function aand
%returns the vector [a,b,R-squared], where yfit=ax+b and R-squared is a
%measure of the goodness of fit.
%It is taken from the following web-page:
http://www.mathworks.se/help/matlab/data_analysis/linear-regression.html

%Fit the data to an n-th order polynomial
p=polyfit(x,y,1);
%a is the slope of the fitted function
a=p(1);
%b is the intercept of the fitted function
b=p(2);

%Produce a vector of coordinates for the fitted function:
yfit=b+a*x;
```

```
%Produce a vector of the residuals
yresid=y-yfit;

%Obtain the residual sum of squares
SSresid=sum(yresid.^2);

%Compute the total sum of squares of y by multiplying the variance of y by
%the number of observations minus one:
SStotal=(length(y)-1)*var(y);

%Compute R-squared:
rsq=1-SSresid/SStotal;

m=[a,b,rsq] ;
end
```

FindPeakmax.m:

```
function [ peak_max_channel, peak_max_counts ] = FindPeakmax( spectra )
%FINDPEAKMAX This function finds the highest point in an LSC spectrum.

[channels,numspectra]=size(spectra);

%Declare empty result arrays:
peak_max_channel=zeros(numspectra,1);
peak_max_counts=zeros(numspectra,1);

%Find the maximum in each spectrum:
for i=1:numspectra
    %Declare zero-values:
    count_max=0;
    channel_max=0;
    %Read the apropriate spectrum from the matrix:
    spectrum=spectra(:,i);
    %Find the maximum in the spectrum:
    for j=1:channels;
        %For each channel, read the number of counts:
        count=spectrum(j);
        %If the count number in the current channel is the highest so far,
        %then store it and the channel number:
        if count>count_max
            count_max=count;
            channel_max=j;
        end
    end
    %Store the maximum channel and counts of the spectrum in the apropriate
    %position in the result arrays:
    peak_max_channel(i)=channel_max;
    peak_max_counts(i)=count_max;
    end
```

Appendix 5: Tables of plotted data

Table 8: The data plotted in Figure 14.

Parallel 1			Parallel 2			Parallel 3		
Channel of peak max	Relative efficiency	SD(Rel E)	Channel of peak max	Relative efficiency	SD(Rel E)	Channel of peak max	Relative efficiency	SD(Rel E)
446	0.996	0.004	449	1.002	0.004	448	1.002	0.004
434	0.986	0.004	430	0.998	0.004	430	0.989	0.004
431	0.977	0.004	423	0.993	0.004	426	0.985	0.004
417	0.985	0.004	414	1.004	0.004	419	0.993	0.004
408	0.987	0.004	398	1.048	0.004	404	1.053	0.004
393	1.024	0.004	391	0.997	0.004	388	1.002	0.004
386	0.999	0.004	379	0.988	0.004	376	0.989	0.004
364	0.986	0.004	350	0.983	0.004	358	0.975	0.004
344	0.971	0.004	345	0.973	0.004	336	0.972	0.004
331	0.966	0.004	330	0.972	0.004	319	0.969	0.004
291	0.942	0.004	283	0.940	0.004	283	0.943	0.004
270	0.937	0.004	275	0.933	0.004	266	0.946	0.004

Table 9: The data plotted in Figure 15.

Parallel 1			Parallel 2			Parallel 3		
Channel of peak max	Relative efficiency	SD(Rel E)	Channel of peak max	Relative efficiency	SD(Rel E)	Channel of peak max	Relative efficiency	SD(Rel E)
446	0.996	0.004	449	1.000	0.004	448	1.004	0.004
434	0.991	0.004	430	1.005	0.004	430	0.995	0.004
431	0.981	0.005	423	0.991	0.004	426	0.984	0.005
417	0.981	0.005	414	0.984	0.005	419	0.979	0.005
408	0.974	0.005	398	0.947	0.005	404	0.955	0.005
393	0.946	0.005	391	0.931	0.005	388	0.936	0.005
386	0.924	0.005	379	0.920	0.005	376	0.924	0.005
364	0.910	0.005	350	0.903	0.005	358	0.902	0.005
344	0.885	0.005	345	0.882	0.005	336	0.883	0.005
331	0.865	0.005	330	0.873	0.005	319	0.872	0.005
291	0.823	0.005	283	0.822	0.005	283	0.825	0.005
270	0.795	0.005	275	0.791	0.005	266	0.806	0.005

Table 10: The data plotted in Figure 16.

Parallel 1			Parallel 2			Parallel 3		
Channel of peak max	Relative efficiency	SD(Rel E)	Channel of peak max	Relative efficiency	SD(Rel E)	Channel of peak max	Relative efficiency	SD(Rel E)
457	1.002	0.004	450	0.989	0.004	455	1.009	0.004
429	1.017	0.004	422	0.980	0.004	427	0.981	0.004
418	0.970	0.004	406	0.957	0.004	411	0.958	0.004
394	0.955	0.004	390	0.942	0.004	389	0.944	0.004
376	0.941	0.004	373	0.932	0.004	377	0.936	0.004
358	0.928	0.004	351	0.925	0.004	350	0.927	0.004
334	0.919	0.004	342	0.920	0.004	337	0.923	0.004
320	0.913	0.004	327	0.907	0.004	334	0.910	0.004
285	0.888	0.004	283	0.894	0.004	285	0.892	0.004
267	0.888	0.004	274	0.883	0.004	274	0.885	0.004
259	0.874	0.004	259	0.879	0.004	277	0.882	0.004
254	0.878	0.004	255	0.878	0.004	267	0.872	0.004
241	0.871	0.004	249	0.873	0.004	253	0.869	0.004
225	0.864	0.004	249	0.866	0.004	241	0.862	0.004
222	0.851	0.004	236	0.850	0.004	239	0.858	0.004
222	0.849	0.004	222	0.861	0.004	226	0.847	0.004
204	0.824	0.004	222	0.838	0.004	222	0.838	0.004
204	0.813	0.004	214	0.829	0.004	222	0.835	0.004

Table 11: The data plotted in Figure 19.

Aliquot 1				Aliquot 2				Aliquot 3			
ml NaOH	pH	ml NaOH	pH	ml NaOH	pH	ml NaOH	pH	ml NaOH	pH	ml NaOH	pH
0	0.49	18.0	1.52	0.0	0.48	21.7	1.86	0.0	0.47	21	1.79
1	0.50	19.4	1.63	1.1	0.51	22.4	1.93	1.0	0.50	22.1	1.9
1.6	0.53	19.7	1.68	2.9	0.58	22.6	1.96	2.0	0.53	22.9	1.99
2.5	0.56	21.5	1.85	4.1	0.63	23.2	2.03	3.0	0.57	23.5	2.08
3.4	0.59	22.2	1.92	5.1	0.68	23.5	2.07	4.1	0.61	24	2.15
4.5	0.64	23.2	2.05	6.4	0.74	24.0	2.13	5.1	0.65	24.5	2.21
6.1	0.72	24.3	2.18	8.1	0.84	24.5	2.19	6.2	0.71	24.9	2.29
7.2	0.77	25.1	2.30	9.2	0.9	24.9	2.24	7.1	0.76	25.3	2.36
8	0.82	26.4	2.55	10.4	0.97	25.4	2.32	8.0	0.81	26	2.48
9	0.88	26.7	2.65	11.6	1.06	25.8	2.39	9.0	0.86	26.5	2.6
10.1	0.94	27	2.75	12.4	1.11	26.3	2.49	10.0	0.93	27	2.73
11.1	1.00	27.7	3.05	13.4	1.17	26.9	2.62	10.9	0.98	27.3	2.87
11.5	1.04	28.2	3.41	15.5	1.25	27.1	2.68	11.9	1.05	27.5	2.95
12.1	1.08	28.4	3.53	15.5	1.32	27.5	2.8	13.2	1.13	27.7	3.03
13	1.14	28.6	3.72	16.5	1.4	27.8	2.92	14.2	1.22	27.9	3.12
14.8	1.26	28.8	3.91	17.1	1.45	28.2	3.13	15.2	1.30	28	3.22
16.5	1.39	28.9	4.05	17.9	1.51	28.5	3.29	16.0	1.36	28.2	3.35
17	1.44			18.5	1.56	28.6	3.44	17.0	1.44	28.4	3.5
				19.3	1.63	28.9	3.77	18.1	1.53	28.5	3.7
				20.4	1.73	29.1	3.94	19.1	1.61	28.6	3.88
				21.2	1.81	29.3	4.07	20	1.7	28.8	4.03

Table 12: The data plotted in Figure 20.

Aliquot 1				Aliquot 2				Aliquot 3			
ml NaOH	pH	ml NaOH	pH	ml NaOH	pH	ml NaOH	pH	ml NaOH	pH	ml NaOH	pH
0	5.84	27.9	6.63	0	5.34	27	5.81	0	5.07	25	5.83
0.3	5.84	28.3	6.67	1	5.33	27.6	5.86	1.2	5.09	26.1	5.9
1.2	5.84	29	6.79	1.9	5.28	28	5.9	2.1	5.12	27	5.98
2.6	5.85	30	7.09	3	5.26	28.5	5.97	3	5.14	28.1	6.1
3	5.86	30.2	7.18	4.1	5.26	29	6.03	4	5.16	29	6.28
4.5	5.87	30.4	7.3	5.3	5.25	29.5	6.16	5	5.17	29.5	6.41
5.4	5.89	30.6	7.58	6.2	5.25	29.9	6.25	6	5.2	30	6.67
6.6	5.91	30.9	8.18	8	5.26	30.2	6.38	7	5.22	30.5	7.3
7.6	5.93	31	8.95	10	5.3	30.7	6.67	8	5.24	30.7	8.01
8.5	5.94	31.15	9.72	11.8	5.32	31	7.12	3.1	5.26	30.8	8.63
9.5	5.96	31.3	10.36	13.4	5.35	31.2	8.45	10	5.29	30.9	9.27
10.4	5.98	31.5	10.7	14.5	5.36	31.4	9.44	11	5.31	31.1	10.01
11.3	5.99	31.8	11.08	15.6	5.39	31.6	10.03	12	5.33	31.25	10.26
11.8	6.01	32.1	11.33	16.9	5.42	31.7	10.25	12.9	5.36	31.4	10.46
12.9	6.04	32.3	11.42	18	5.44	32	10.61	14	5.38	31.6	10.66
15.1	6.09	33.2	11.66	19.1	5.47	32.3	10.85	15	5.42	31.8	10.89
16.1	6.11	34	11.75	20.1	5.5	32.8	11.02	16	5.45	32.1	10.99
17.6	6.15	35	11.84	21.1	5.53	33.7	11.25	17	5.49	32.3	11.08
19.3	6.2	36	11.88	22.4	5.57	34.5	11.35	18	5.51	33	11.22
21	6.25	37	11.92	23.2	5.6	35.5	11.42	19	5.55	34	11.31
22.6	6.32	38.1	11.95	24.3	5.65	37	11.47	20	5.59	35	11.36
23.5	6.36	39	11.97	25.5	5.72	38.5	11.51	21	5.62	36	11.4
25.8	6.46	40.3	12	26.4	5.78	40.1	11.54	22	5.67	37	11.41
26.1	6.47	41.1	12.02					23	5.71	38.5	11.43
26.8	6.53	42	12.04					24	5.76	40	11.45

Table 13: The data plotted in Figure 21.

pH	Distribution ratio (D)	Standard deviation of D
0.93	0.005	0.002
1.11	0.0091	0.0002
2.00	0.71	0.03

Table 14: The data **plotted in Figure 22.**

Stirring time (minutes)	Percent extracted %E	Standard deviation of %E
2	5.7	0.1
10	5.9	0.1
15	5.9	0.6
30	6.5	0.1
60	5.4	0.1

Table 15: The data plotted in Figure 23.

Shaking time (minutes)	Percent extracted %E	Standard deviation of %E
5	72	2
10	72	2
30	73.1	0.4

Table 16: The data plotted in Figure 24.

pH	Distribution ratio (D)	Standard deviation of D
0.30	0.0061	0.0002
1.10	0.165	0.003
1.45	0.82	0.02
2.00	8.0	0.2

Table 17: The data plotted in Figure 25.

HDEHP concentration (M)	Distribution ratio (D)	Standard deviation of D
0.1	0.023	0.001
0.25	0.165	0.003
0.5	0.75	0.02
1	2.6	0.2

Table 18: The data plotted in Figure 26.

1 M HDEHP		
pH	Distribution ratio (D)	Standard deviation of D
1.1	0.165	0.003
1.5	0.82	0.02
2.0	7.99	0.16
0.3	0.0061	0.0002
0.5 M HDEHP and 0.5 M TBP		
1.1	0.0105	0.0002
1.5	0.047	0.003
2	0.94	0.04
0.2 M HDEHP		
0.9	0.001	0.001
1.1	0.0059	0.0003
2	0.71	0.03

Table 19: The data plotted in Figure 28.

pH	Distribution ratio (D)	Standard deviation of D
0.3	$6 \cdot 10^2$	$2 \cdot 10^2$
0.9	$7 \cdot 10$	3
1.1	$3 \cdot 10$	2
2.0	1.8	2

Table 20: The data plotted in Figure 29

pH	Distribution ratio (D)	Standard deviation of D
0.4	$3.3 \cdot 10^2$	$6 \cdot 10$
0.9	$1.2 \cdot 10^2$	$3 \cdot 10$
1.4	30	5
1.1	$4 \cdot 10$	$3 \cdot 10$
2.0	12	3

Table 21: The data plotted in Figure 30.

Concentration of Cyanex 301 (M)	Distribution ratio (D)	Standard deviation of D
0.016	$4 \cdot 10^2$	$1 \cdot 10^2$
0.155	7	1
0.775	1.4	0.1
0.004	$1.4 \cdot 10^2$	$7 \cdot 10$
0.039	16	4
0.388	3.3	0.6

Bibliography

1. *The Lund/LBNL Nuclear Data Search (http://nucleardata.nuclear.lu.se/toi/index.asp); Retrieved 19.03.2014*.

2. *Global agriculture towards 2050*. 2009, Food and Agriculture Organization of the United Nations: Rome.

3. Scherer, H.W., K. Mengel, G. Kluge, and K. Severin, *Fertilizers, 1. General*, in *Ullmann's Encyclopedia of Industrial Chemistry*. 2000, Wiley-VCH Verlag GmbH & Co. KGaA.

4. Stewart, W.M. and T.L. Roberts, *Food Security and the Role of Fertilizer in Supporting it.* Procedia Engineering, 2012. **46**(0): p. 76-82.

5. Kongshaug, G., B.A. Brentnall, K. Chaney, J.-H. Gregersen, P. Stokka, B. Persson, N.W. Kolmeijer, A. Conradsen, T. Legard, H. Munk, and Ø. Skauli, *Phosphate Fertilizers*, in *Ullmann's Encyclopedia of Industrial Chemistry*. 2000, Wiley-VCH Verlag GmbH & Co. KGaA.

6. Gilbert, N., *Environment: The disappearing nutrient*, in *Nature News*. 2009, Nature Publishing Group. p. 716-718.

7. Nogawa, K. and Y. Suwazono, *Itai-Itai Disease*, in *Encyclopedia of Environmental Health*, J.O. Nriagu, Editor. 2011, Elsevier: Burlington. p. 308-314.

8. Butusov, M. and A. Jernelöv, *Phosphorus: An Element that could have been called Lucifer*. 2013, New York, NY: Springer New York. IX, 101 s. 27 illus., 17 illus. in color. : digital.

9. Appl, M., *Ammonia*, in *Ullmann's Encyclopedia of Industrial Chemistry*. 2000, Wiley-VCH Verlag GmbH & Co. KGaA. p. 121.

10. Lamichhane, K.M. and R.W. Babcock Jr, *Survey of attitudes and perceptions of urine-diverting toilets and human waste recycling in Hawaii.* Science of The Total Environment, 2013. **443**(0): p. 749-756.

11. Morton, B., *Reclaiming minerals from waste water to make fertilizer.* The Vancouver Sun. Retrieved September 18th, 2013, 2013.

12. Harris, D.C., *Quantitative Chemical Analysis*. 2003, New York: W.H Freeman and Company.

13. Lerum, H.V., *Sketch of a cyclotron. Personal communication with H. Kristiansen*. 2014.

14. Xiaolong, H., Y. Shenggui, and D. Chunsheng, *Evaluation of the decay data of 109Cd.* Nuclear Instruments and Methods in Physics Research Section A: Accelerators, Spectrometers, Detectors and Associated Equipment. **621**(1–3): p. 443-446.

15. Lehto, J. and X. Hou, *Chemistry and analysis of radionuclides: laboratory techniques and methodology*. 2011, Weinheim: Wiley. XIX, 406 s. : ill.

16. Guin, R., S.K. Saha, S. Prakash, and M. Uhl, *Isomeric yield ratios and excitation functions in α-induced reactions on 107,109Ag.* Physical Review C, 1992. **46**(1): p. 250-257.

17. Chaubey, A.K., M.K. Bhardwaj, R.P. Gautam, R.K.Y. Singh, M. Afzal Ansari, I.A. Rizvi, and H. Singh, *Pre-Equilibrium Decay Process in the Alpha Induced Reactions of Silver Isotopes.* Applied Radiation and Isotopes, 1990. **41**.

18. Peng, X., X. Long, F. He, and M. Liu, *Excitation functions and yields of the reactions induced by alpha-particle bombardment of natural silver.* Applied Radiation and Isotopes, 1996. **47**(3): p. 309-313.

19. Porges, K.G., *Alpha Excitation Functions of Silver and Copper.* Physical Review, 1956. **101**(1): p. 225-230.

20. Rydberg, J., *Solvent extraction principles and practice*. 2nd ed., rev. and expanded. ed. 2004, New York: Marcel Dekker.

21. Touati, M., M. Benna-Zayani, N. Kbir-Ariguib, M. Trabelsi-Ayadi, A. Buch, J.L. Grossiord, D. Pareau, and M. Stambouli, *Extraction of Cadmium from Phosphoric Acid Media by Di(2-ethylhexyl) Dithiophosphoric Acid.* Solvent Extraction and Ion Exchange, 2008. **26**(4): p. 420-434.

22. Jha, M.K., V. Kumar, J. Jeong, and J.-C. Lee, *Review on solvent extraction of cadmium from various solutions.* Hydrometallurgy, 2012. **111 112**: p. 1.

23. Mellah, A. and D. Benachour, *The solvent extraction of zinc and cadmium from phosphoric acid solution by di-2-ethyl hexyl phosphoric acid in kerosene diluent.* Chemical Engineering and Processing: Process Intensification, 2006. **45**(8): p. 684-690.

24. Mellah, A. and D. Benachour, *The solvent extraction of zinc, cadmium and chromium from phosphoric acid solutions by tri-n butyl phosphate in kerosene diluent.* Separation and Purification Technology, 2007. **56**(2): p. 220-224.

25. Reddy, B.R.P., D. Neela, *Chloride leaching and solvent extraction of cadmium, cobalt and nickel from spent nickel–cadmium, batteries using Cyanex 923 and 272.* Journal of Power Sources, 2006.

26. Nikam, G., K. Mahanwar, S. Sabale, and B. Mohite, *Extractive Separation of Cadmium(II) using Cyanex 923 from Ammonium Thiocyanate Medium.* Separation Science and Technology, 2012. **48**(3): p. 493-500.

27. *Technical brochure for Cyanex 301 Extractant*. Cytec Industries Inc.

28. Ocio, A., A. Almela, and M.P. Elizalde, *Cadmium(II) Extraction from Phosphoric Media by bis(2,4,4-Trimethylpentyl)dithiophosphinic Acid (CYANEX 301).* Solvent Extraction and Ion Exchange, 2004. **22**(6): p. 961-977.

29. Brown; Timothy J., R.W.A., Boyle; Richard J., *Selective removal of metals from aqueous solutions with dithiophosphinic acids, US Patent 7,721,605*. 1985.

30. Sole, K.C., J. Brent Hiskey, and T.L. Ferguson, *An assessment of the long-term stabilities of Cyanex 302 and Cyanex 301 in sulfuric and nitric acids.* Solvent Extraction and Ion Exchange, 1993. **11**(5): p. 783-796.

31. Marc, P., R. Marc, G. Custelcean, J. Groenewold, D. Klaehn, L. Peterman, and Delmau, *Degradation of Cyanex 301 in Contact with Nitric Acid Media.* Industrial & engineering chemistry research, 2012. **51**(40): p. 13238-13244.

32. *Personal communication betweenCyril Bourget, MEP Account Manager for Europe and Northern Africa, CYTEC Industries France SARL and Håvard Kristiansen, Graduate Student, University of Oslo*. 2015.

33. Jean-Jacques Robert Perraud, Mississauga; Dennis Frederick Colton, Carlisle; Jean Paul Duterque, and Oakville; Yoshiaki Okita, *Hydrogen-free regeneration of dithiophosphorus metal extractants*. 2000: USA. p. 7.

34. Kossert, K.O., O; Nähle, O, *Improved techniques for the activity standardization of 109Cd by means of liquid scintillation spectrometry.* LSC 2008, Advances in Liquid Scintillation Spectrometry, 2009.

35. Takeshita, K., K. Watanabe, Y. Nakano, and M. Watanabe, *Solvent extraction separation of Cd(II) and Zn(II) with the organophosphorus extractant D2EHPA and the aqueous nitrogen-donor ligand TPEN.* Hydrometallurgy, 2003. **70**(1-3): p. 63-71.

36. Eriksen, D., *Personal communication with H. Kristiansen.* 2015.